

Dynamics and rheology of semidilute solutions of ring-linear polymer blends in planar extensional flow

Charles D. Young,^{1,2} Yuecheng Zhou,^{3,2, a)} Charles M. Schroeder,^{3,1,2} and Charles E. Sing^{1,2, b)}

¹⁾*Department of Chemical and Biomolecular Engineering, University of Illinois at Urbana-Champaign, Urbana, Illinois 61801, USA*

²⁾*Beckman Institute for Advanced Science and Technology, University of Illinois at Urbana-Champaign, Urbana, IL, 61801*

³⁾*Department of Materials Science and Engineering, University of Illinois at Urbana-Champaign, Urbana, Illinois 61801, USA*

(Dated: 26 May 2022)

We use Brownian dynamics (BD) simulations and single molecule experiments to investigate the influence of topological constraints and hydrodynamic interactions on the dynamics and rheology of solutions of ring-linear polymer blends at the overlap concentration. We find agreement between simulation and experiment in that rings in solution blends exhibit large conformational fluctuations, including extension overshoots on the startup of flow and tumbling and tank-treading at steady state. Ring polymer fluctuations increase with blend fraction of linear polymers and are peaked at a ring Weissenberg number $Wi_R \approx 1.5$. On the contrary, linear and ring polymers in their pure solution show a peak in fluctuations at the critical coil-stretch Weissenberg number $Wi = 0.5$. BD simulations show that extension overshoots on startup of flow are due to flow-induced intermolecular ring-linear polymer hooks, whereas fluctuations at steady state are driven by intermolecular hydrodynamic interactions (HI). The streamlines determined from BD simulation are qualitatively comparable to elastic instabilities in cross-slot flow of polymer solutions, and we speculate that the dynamics of solution blends may be understood by deviations of the flow from planar extension. This is supported by simulations of bidisperse linear polymer solution blends, which show similar trends in conformational dynamics between rings and linear polymers with a matched contour length. Comparing to BD simulations, single molecule experiments show quantitatively larger fluctuations, which could arise because experiments are performed on higher molecular weight polymers with stronger entanglement effects. To this end, we have advanced the understanding of the effects of topological interactions and intermolecular HI on the dynamics of semidilute ring-linear polymer blend solutions.

I. INTRODUCTION

The dynamics of ring polymers are of broad interest to fundamental polymer physics,^{1,2} technological applications,^{3,4} and biological systems.⁵ In the context of polymer physics, ring polymers are a model for understanding the effect of chain architecture. The dynamics and rheology of linear polymer solutions at varying concentration have been widely studied.^{6,7} In the dilute limit, dynamics are governed by intramolecular excluded volume (EV) and hydrodynamic interactions (HI). Polymer solutions enter the semidilute regime above the overlap concentration $c^* = M/(N_A R_g^3)$, where M is the polymer molecular weight, N_A is Avogadro's number, and R_g is the dilute polymer radius of gyration. In semidilute solutions, polymer dynamics are determined by both intra- and intermolecular EV and HI. Finally, in melt EV and HI are fully screened, and polymer dynamics are well described by either the Rouse model for unentangled polymers or the tube-reptation model for entangled polymers. The introduction of an end-free constraint in ring polymers, however, changes the conformational dynamics and

rheology of polymers in all three concentration regimes qualitatively and quantitatively.

In melt, polymer rheology can largely be understood on the basis of topological constraints. Linear polymer melts relax stress by reptation of free ends along the polymer backbone, leading to a rubbery plateau modulus.^{6,7} However, in ring polymer melts the end-free constraint significantly suppresses entanglements and drives rings toward globular conformations, resulting in a significantly lower zero-shear viscosity as compared to linear polymer melts and the absence of a rubbery plateau modulus.⁸⁻¹⁰ Thus, ring polymers are an appealing option for applications requiring high polymer mass transport but low viscosity. These results are only valid for pure ring melts, which remain challenging to synthesize.^{11,12} The introduction of even trace linear contaminants results in significantly higher zero-shear viscosity and the return of a rubbery plateau modulus.^{8,9} These rheological features are intrinsically connected to the polymer dynamics. Molecular dynamics (MD) simulations show long-lived relaxation modes in ring-linear polymer melt blends associated with the threading of linear polymers through rings.¹³ MD simulations also show a maximum in zero-shear viscosity as a function of blend ratio at $\phi_{linear} = 0.5$ (where ϕ_{linear} is the linear polymer weight fraction) due to ring-linear threading.⁹

Polymer processing generally involves strong flows,

^{a)}Current address: Department of Chemistry, Stanford University, Stanford, California 94305, USA

^{b)}Electronic mail: cesing@illinois.edu

where the coupling of architecture and deformation complicate the idea of suppressed entanglements in pure ring melts. Filament stretching rheometry has shown that ring polymer melts in uniaxial extensional flow thicken at unexpectedly low strain rates,¹⁴ a phenomenon which has been shown by MD simulations to be caused by topological linking.¹⁵ Ring linking has also been observed in melts under shear, although the effects on shear viscosity are less pronounced than in extension.^{9,16,17} The effect of blend ratio is also relevant in flow. MD simulations show the shear viscosity is independent of blend ratio when melts are exposed to high shear rates,⁹ but there may be stronger effects in extension.

In contrast to melts, entanglement effects are weaker in solutions;^{6,7} the coupling of HI and EV to polymer architecture becomes important, particularly in strong flows.^{18,19} In the dilute limit, equilibrium ring polymer dynamics and conformations have been widely studied by single molecule experiments,²⁰ theory,²¹ and simulation.²² In planar extensional flow, ring polymers exhibit a delayed coil-stretch transition due to intramolecular hydrodynamics which drive the ring to stretch in the flow-neutral direction into an open loop conformation.^{23,24} In shear flow, rings undergo ‘end-over-end’ tumbling as observed in linear polymers,²⁵ as well as tank-treading dynamics as seen in vesicles.^{26,27} In the more general case of mixed flows, rings exhibit both tumbling and stretching behavior.²⁸ Overall, rings in dilute solution demonstrate unique conformational dynamics and quantitatively different rheological responses as compared to linear polymers.

Semidilute polymer solutions incorporate the physics of both the melt and dilute regimes, namely entanglement or topological constraints and intra and intermolecular interactions due to excluded volume and solvent-mediated hydrodynamics.^{6,7} At equilibrium, the influence of chain architecture in pure solution is primarily quantitative, as ring and linear polymers demonstrate similar scaling of dynamic and static properties with concentration and molecular weight.²⁹ However, blends of ring and linear polymers in semidilute solution can display qualitatively different dynamics, particularly above the entanglement concentration c_e as traditionally defined for linear polymers.⁷ Single molecule studies on the diffusion of trace rings in a background of semidilute linear polymers have shown a scaling with concentration lower than that of the pure linear solution prediction, suggesting ring-linear threading inhibits ring diffusion in a manner not described by reptation theories.³⁰ Further studies found that as the blend fraction of ring polymers decreased from a primarily ring to primarily linear polymer solution, the diffusion of ring polymers decreased markedly.³¹ Monte Carlo simulations found good qualitative agreement with this trend, attributing the slower dynamics to ring-linear threading.³¹ This is supported by MD melt simulations, which show that ring-ring threadings are significantly less probable and have a weaker effect on ring dynamics as compared to ring-linear

threads.¹⁶ Notably, slow ring dynamics are most apparent above the entanglement concentration c_e , which for the 45 kbp DNA used is related to the overlap concentration as $c_e \approx 3 c^*$.^{32,33} At lower concentrations, the dependence on blend fraction is less pronounced.³¹

However, the flow dynamics of semidilute solutions of pure rings or ring-linear polymer blend is still not well understood. In particular, it is not clear if the application of flow introduces topological constraints or strong solvent-mediated HI which are absent at equilibrium. Recently, Zhou et al. performed single molecule experiments on ring polymers trapped at the stagnation point of planar extensional flow in background solutions of linear polymers at $0.025 c^*$, $0.1 c^*$, and $1 c^*$.³⁴ At $0.025 c^*$, ring polymer conformational fluctuations were peaked at $Wi_R \approx 0.5$, where Wi_R is the dimensionless flow strength on trace ring polymers defined as $Wi_R = \dot{\epsilon} \tau_R$, $\dot{\epsilon}$ is the strain rate, and τ_R is the longest relaxation time of the trace ring polymer. This is in agreement with the expectation that conformational fluctuations are largest at the critical coil-stretch transition flow rate, which is supported by previous experiments and simulations on semidilute linear polymer solution^{35–38}, and dilute linear and ring polymer solution.^{23,24,28} At $0.1 c^*$, however, the maximum conformation fluctuation was shifted to $Wi_R \approx 0.9$, with only a weak decrease thereafter. Approaching the semidilute regime at $1 c^*$, fluctuations increased up to $Wi_R \approx 1.5$ and then plateaued. These results raise questions regarding the nature of intermolecular interactions in non-dilute ring-linear polymer blends.

Single molecule experiments and simulations of linear semidilute polymer solutions have already suggested plausible explanations. At $1 c^*$, slow-stretching and fast-stretching end-coiled sub-populations emerge upon the startup of planar extensional flow, leading to broader conformational distributions as compared to dilute solutions.^{35,36} The authors suggested this could be due to flow induced intermolecular hooks which form between folded and end-coiled conformations. In the current study, we performed Brownian dynamics (BD) simulations at similar conditions and observed both broader conformational distributions at $1 c^*$ and transient intermolecular hooks, although rarely found at $1 c^*$.³⁸ Simulations also revealed a population of linear polymers which interconverted between coiled and stretched states at moderate flow rates $Wi_L \approx 1.5$, whereas linear polymers in dilute solution have already stretched under such flow rate.^{38,39} The slow stretching dynamics and retraction were assigned to intermolecular hydrodynamic interactions (HI), but a more detailed study was deferred.

Past molecular simulation studies of semidilute polymer solutions in flow have focused on molecular scale physics.^{36–38,40,41} However, the modification of applied flow in viscoelastic liquids due to the elastic stress may be relevant to polymer dynamics. The nonlinear stress term in polymer solutions can cause striking changes in flow behavior.⁴² With respect to the current study at negligible Reynolds number, purely elas-

tic instabilities arise from normal stress differences along curved streamlines.^{43,44} Particle tracking velocimetry experiments and continuum simulations of unentangled polymer solution flow in cross-slot microfluidic devices have shown elastic instabilities associated with the extra polymer stress.^{45,46} As the flow strength increases above $Wi \approx 0.5$, the polymer disturbance to the flow causes stagnation point displacement, steady asymmetric flow across the axis of extension, and unsteady mixed flows.^{47,48} BD simulations of dilute polymer solutions in mixed flows show broad conformational distributions as polymers can tumble as in shear and stretch as in extension.^{28,49} Thus, elastic instabilities may be relevant to microscopic polymer dynamics, although the connection is not clear for semidilute polymer solutions under straining flows.

In this work, we combine BD simulations and single molecule experiments to study the influence of planar extensional flow and blend composition in semidilute solutions of ring-linear polymer blends. We consider solutions at the overlap concentration c^* while increasing flow rate through the coil-stretch transition with $Wi_R = 0.4 - 3.2$ and varying the blend composition from a *pure ring polymer solution to a trace ring in linear polymer background solution*. The article is organized as follows: In Sec. II we describe the simulation method and experimental procedure. In Sec. III we quantify the conformational dynamics and solution rheology. Ring polymers are found to exhibit large conformational fluctuations which are sensitive to the blend ratio. We further investigate the origin of ring conformational fluctuations in Sec IV. We find that intermolecular ring-linear polymer hooks lead to overshoots in ring extension on startup of flow, and intermolecular HI lead to large fluctuations in extension at steady state. Finally, we summarize our results and highlight topics for future studies in Sec. V.

II. METHODS

A. Simulation Governing Equations

We perform BD simulations of semidilute ring-linear polymer blend solutions in a planar extensional flow. The simulations consists of n_R ring polymers and n_L linear polymers each with the same number of coarse-grained beads per chain $N_R = N_L = 150$. The total number of beads is then $N = n_R N_R + n_L N_L$. The position \mathbf{r}_i of a bead i is updated according to the Langevin equation

$$\frac{d\tilde{\mathbf{r}}_i}{dt} = \tilde{\boldsymbol{\kappa}} \cdot \tilde{\mathbf{r}}_i - \sum_j \tilde{\mathbf{D}}_{ij} \nabla_{\tilde{\mathbf{r}}_j}(\tilde{U}) + \tilde{\boldsymbol{\xi}}_i \quad (1)$$

Tildes denote dimensionless quantities. Positions are normalized by the bead radius ($\tilde{\mathbf{r}} = \mathbf{r}/a$), energies are normalized by the thermal energy $k_B T$ ($\tilde{U} = U/(k_B T)$), times are normalized by the single-bead diffusion time ($\tilde{t} = t/\tau_0$, where $\tau_0 = 6\pi\eta_s a^3/(k_B T)$ and η_s is the solvent viscosity), and the diffusion tensor is normalized

by the drag coefficient of the spherical polymer beads ($\tilde{\mathbf{D}}_{ij} = \mathbf{D}_{ij}(6\pi\eta a/(k_B T))$). Polymer beads experience flow via the $3N \times 3N$ block diagonal tensor $\tilde{\boldsymbol{\kappa}}$, which has 3×3 diagonal blocks given by the solvent velocity gradient tensor $(\nabla\tilde{\mathbf{v}})^T$. For planar extensional flow,

$$\nabla\tilde{\mathbf{v}} = \begin{pmatrix} \tilde{\epsilon} & 0 & 0 \\ 0 & -\tilde{\epsilon} & 0 \\ 0 & 0 & 0 \end{pmatrix} \quad (2)$$

where $\tilde{\epsilon} = \dot{\epsilon}\tau_0$ is the dimensionless strain rate. Beads interact via a potential $\tilde{U} = \tilde{U}^B + \tilde{U}^{EV}$ consisting of bonded and excluded volume contributions. We use a finitely extensible non-linear elastic (FENE) spring force for connectivity

$$\tilde{U}^B = -0.5\tilde{k}_s\tilde{r}_{max}^2 \ln \left[1 - \left(\frac{\tilde{r}_{ij}}{\tilde{r}_{max}} \right)^2 \right] \quad (3)$$

where $\tilde{k}_s = 30\tilde{u}/\tilde{\sigma}^2$ is the spring constant, $\tilde{u} = 1.0$ gives the strength of EV interactions, and $\tilde{\sigma} = 2$ is the diameter of a bead. The maximum extension of a spring is $\tilde{r}_{max} = 1.5\tilde{\sigma}$, and \tilde{r}_{ij} is the distance between two connected beads. Excluded volume interactions are modeled by a shifted, purely repulsive Lennard-Jones potential

$$\tilde{U}^{EV} = 4\tilde{u} \left[\left(\frac{\tilde{\sigma}}{\tilde{r}_{ij}} \right)^{12} - \left(\frac{\tilde{\sigma}}{\tilde{r}_{ij}} \right)^6 + \frac{1}{4} \right] \Theta(2^{1/6}\tilde{\sigma} - \tilde{r}) \quad (4)$$

which yields chain statistics representative of a good solvent. We find $\nu \approx 0.59$ from the scaling relation $\tau_Z \sim N^{3\nu}$ and relaxation time data from equilibrium single chain simulations, in agreement with the result for a polymer in good solvent.^{6,7} This model has been widely utilized to study polymer dynamics in solution and melt and has been shown to prevent chain crossings in simulations of entangled melts in extensional flow.⁵⁰

Solvent-mediated HI and Stokes drag are included via the diffusion tensor, given here by the Rotne-Prager Yamakawa (RPY) tensor,^{51,52}

$$\tilde{\mathbf{D}}_{ij} = \begin{cases} \mathbf{I}, & i = j \\ \frac{3}{4\tilde{r}_{ij}} \left[\left(1 + \frac{2}{3\tilde{r}_{ij}^2} \right) \mathbf{I} + \left(1 - \frac{2}{\tilde{r}_{ij}^2} \right) \hat{\mathbf{r}}_{ij}\hat{\mathbf{r}}_{ij} \right], & i \neq j, \tilde{r}_{ij} \geq 2 \\ \left(1 - \frac{9\tilde{r}_{ij}}{32} \right) \mathbf{I} + \frac{3\tilde{r}_{ij}}{32} \hat{\mathbf{r}}_{ij}\hat{\mathbf{r}}_{ij}, & i \neq j, \tilde{r}_{ij} \leq 2 \end{cases} \quad (5)$$

$\hat{\mathbf{r}}_{ij} = \tilde{\mathbf{r}}_{ij}/r_{ij}$ is a unit vector in the direction of $\tilde{\mathbf{r}}_{ij} = \tilde{\mathbf{r}}_j - \tilde{\mathbf{r}}_i$ and \mathbf{I} is the identity matrix. The average and first moment of the Brownian noise $\tilde{\boldsymbol{\xi}}_i$ are given by the fluctuation-dissipation theorem as $\langle \tilde{\boldsymbol{\xi}}_i(t) \rangle = 0$ and $\langle \tilde{\boldsymbol{\xi}}_i(t)\tilde{\boldsymbol{\xi}}_j(t') \rangle = 2\tilde{\mathbf{D}}_{ij}\delta(t-t')$ respectively. Simulation implementation requires the decomposition of the diffusion tensor as $\tilde{\mathbf{D}} = \tilde{\mathbf{B}}\tilde{\mathbf{B}}^T$ so that the Brownian noise can be computed via $\tilde{\boldsymbol{\xi}}_i = \sqrt{2}\tilde{\mathbf{B}}_{ij}\mathbf{f}_j$, where \mathbf{f}_j is a Gaussian random variable with mean 0 and variance dt . In traditional BD simulations, evaluation of the Brownian noise is a computational bottleneck, with the cost scaling as

$O(N^2) - O(N^3)$ depending on the algorithm.^{53–55} To bypass this expense, we use the iterative conformational averaging (CA) method. A brief description of the method and extension to the case of ring-linear polymer blends is given in Section II B, and a more detailed derivation and verification can be found in the authors' previous work.^{38,56,57}

Polymers are simulated in an initially rectangular simulation cell of volume $\tilde{V} = \tilde{l}_x \tilde{l}_y \tilde{l}_z$. The initial cell dimensions in the extension and compression directions are \tilde{l}_x and \tilde{l}_y respectively which must be equal due to the use of Kraynik-Reinelt boundary conditions for deformation of the box with the flow.^{58,59} We specify the cell size in the neutral direction \tilde{l}_z to be smaller than \tilde{l}_x and \tilde{l}_y so that the cell dimension in the extension direction is larger. This reduces finite size effects arising from polymers interacting with their own periodic images. A similar approach has been used in simulations of polymer melts in planar extensional flow, which found that results from the rectangular cell simulation were in quantitative agreement with results from a cubic box simulation.⁶⁰ The cell volume is determined by $\tilde{V} = N/\tilde{c}$, where \tilde{c} is the polymer concentration. We set the concentration via the normalized value \tilde{c}/\tilde{c}_L^* , where $\tilde{c}_L^* = N_L/(4/3\pi\langle\tilde{R}_{g0,L}\rangle^3)$ is the overlap concentration. This defines the overlap with respect to the dilute linear polymer radius of gyration $\langle\tilde{R}_{g0,L}\rangle$. We have adopted this definition for consistency with the single molecule experiments.³⁴ As a result, the effective normalized concentration decreases with increasing ring polymer blend fraction due to the smaller radius of gyration of the ring. The difference between the equilibrium sizes of ring and linear polymers is considerable ($\langle\tilde{R}_{g0,L}\rangle = 19.5$ vs $\langle\tilde{R}_{g0,R}\rangle = 14.5$), suggesting a change in the effective concentration may be important. However, we have performed simulations of pure ring polymer solutions at \tilde{c}_R^* based on the ring polymer radius of gyration and found the results to be nearly quantitatively consistent with those presented here for $f_R = 1$, which use $\tilde{c}/\tilde{c}_L^* = 1.0$, $\tilde{c}/\tilde{c}_R^* = 0.4$. All following references to the overlap concentration c^* indicate the value for the pure linear solution \tilde{c}_L^* , and tildes are dropped because only the normalized concentration is used.

We consider solution blends at the overlap concentration c^* for a range of linear polymer fractions $f_R = 0.02 - 1$ and flow rates $Wi_R = 0.4 - 3.2$. The ring polymer fraction controls the blend ratio and is defined as $f_R = n_R/(n_R + n_L)$. We define the ring polymer Weissenberg number $Wi_R = \epsilon\tau_R$, where τ_R is the longest ring linear polymer relaxation time. We consider the single exponential ring relaxation time at the relevant blend fraction, which is determined as described in Section III B. The number of polymers in the simulation box and the resulting box dimensions are given in Table I. Note that simulations at $f_R = 0.02$ use a smaller box size for computational efficiency, as only one ring polymer trajectory is gathered per simulation run. We have also performed $n_{run} = 3$ simulation runs at $f_R = 0.01$ using the same larger box dimensions as for $f_R = 0.17 - 0.83$.

We find the linear polymer dynamics agree quantitatively between the larger and smaller boxes, so to study ring polymer dynamics we use the latter. A smaller simulation box size is also used for $f_R = 1$ because the contour length of ring polymers is half that of linear polymers.

Polymer conformations are initialized following a procedure inspired by simulation of ring-linear polymer blend melts.⁹ Rings are introduced as randomly oriented circular ellipses on a square lattice with spacing greater than the diameter of the rings. This ensures that rings are initially non-concatenated. The number of beads is generally greater than intended because the box is cubic and the lattice is filled. Rings are randomly removed until the target number of beads N is reached. Rings are then relaxed from their circular conformations in a freely draining (FD) simulation for a duration τ_R^{FD} corresponding to the FD ring relaxation time determined from dilute solution FD simulations. At this point, the concentration is lower than intended due to the large initial lattice spacing, so we decrease the box size to the target dimensions. The ring polymers are further relaxed for $10\tau_R^{FD}$ before n_L rings are removed and replaced with random-walk non-overlapping linear polymers to reach the target blend ratio. Finally, the system is allowed to relax for another $10\tau_L^{FD}$ corresponding to the dilute solution FD linear polymer relaxation time.

By this procedure, we aim to reach an accurate equilibrium conformation for a ring-linear polymer blend solution. As discussed in Section IV A, the initial probability of a linear polymer threading a ring is of significant importance to the transient dynamics on startup of flow. Unfortunately, simulation studies on the equilibrium conformations, dynamics, and threading probability of ring-linear polymer blends in solution are limited, and existing results focus on concentrations $c > c_e$. The problem of dynamics is particularly challenging because of the need to accurately resolve solvent-mediated HI. The polymer density at c^* is relatively low ($\rho = N/V = 0.04/\sigma^3$), so we assume that our procedure provides accurate equilibrium conformations and continue to out-of-equilibrium dynamics and rheology, which are the focus of this work.

Initialization is followed by a production run including flow and HI. Kraynik-Reinelt boundary conditions (KRBCs)⁵⁸ are implemented such that the simulation cell deforms consistently with the applied flow. We follow the algorithm of Todd and Daivis,⁵⁹ which allows for unrestricted strain accumulation. Hydrodynamics are accounted for using an Ewald sum,^{61,62} which overcomes the slow convergence of the RPY tensor by splitting the sum into exponentially decaying real space and reciprocal space parts. Excluded volume interactions are accelerated using a cell list generalized for homogeneous linear 3D flow.⁶³ As the simulation progresses, the accumulated Hencky strain is given by the applied flow rate $\epsilon_H = \epsilon t$. We simulate until a total strain $\epsilon_{tot} = 15 - 20$, after which flow is halted and the box remains in the conformation at the cessation flow time $t_{cess} = \epsilon_{tot}/\dot{\epsilon}$. We then simu-

f_R	n_R	n_L	\tilde{l}_x, \tilde{l}_y	\tilde{l}_z	n_{run}
1	34 – 64	0	108.3 – 148.5	90.0	3
0.83	61 – 106	13 – 22	151.1 – 199.3	100.0	3
0.5	37 – 64	37 – 64	151.1 – 199.3	100.0	3
0.17	13 – 22	61 – 106	151.1 – 199.3	100.0	3 – 5
0.02	1	39 – 62	124.6 – 156.3	80.0	40

TABLE I. Simulation parameters for each blend ration f_R . n_R is the number of rings polymers. n_L is the number of linear polymers. \tilde{l}_x, \tilde{l}_y , and \tilde{l}_z are the initial simulation box dimensions in the extension, compression, and neutral directions respectively. n_{run} is the number of simulation runs. The low end of the range corresponds to simulations at a flow rate $Wi_R = 0.4$, and the high end corresponds to simulations at $Wi_R = 0.8, 1.6, 3.2$.

late relaxation dynamics for $10\tau_L^{FD}$. The simulation is advanced by explicit Euler integration of the Langevin equation using a time step of $dt = 5 \times 10^{-4}\tau_0$.

B. Iterative conformational averaging method

We follow the approach of Geyer and Winter, who introduced the truncated expansion ansatz (TEA) approximation to the correlated Brownian noise.⁶⁴ The CA method introduces two further assumptions: (i) the decomposition coefficients of the TEA are conformationally averaged (ii) for interparticle distances above a cutoff \tilde{r}_c , the RPY tensor is discretely evaluated on a grid. The Langevin equation then becomes

$$\frac{d\tilde{\mathbf{r}}_i^{(w)}}{dt} = \tilde{\boldsymbol{\kappa}} \cdot \tilde{\mathbf{r}}_i^{(w)} - \sum_j \tilde{\mathbf{D}}_{ij}^{eff} \nabla_{\tilde{\mathbf{r}}_j}(\tilde{U}) + \tilde{\boldsymbol{\xi}}_i^{(w)}(\epsilon_o) \quad (6)$$

where the superscript (w) denotes the iteration number. The diffusion tensor is approximated by an exact Ewald sum within a cutoff radius $\tilde{r}_c = 12a$ and a discrete approximation to the RPY tensor outside the cutoff

$$\tilde{\mathbf{D}}_{ij}^{eff} = \tilde{\mathbf{D}}_{ij}^{RPY} \Theta(\tilde{r}_c - \tilde{r}_{ij}) + \tilde{\mathbf{D}}_{ij}^G(t) \Theta(\tilde{r}_{ij} - \tilde{r}_c) \quad (7)$$

The *RPY* superscript indicates the full Ewald sum and the *G* the discrete grid space approximation, given by $\tilde{\mathbf{D}}_{ij}^G = \tilde{\mathbf{D}}^{RPY}(\Delta\tilde{\mathbf{r}}_{ij})$, where $\Delta\tilde{\mathbf{r}}_{ij} = (\Delta\tilde{x}_{ij}, \Delta\tilde{y}_{ij}, \Delta\tilde{z}_{ij})$ is the pair displacement rounded to the nearest grid point. We use a grid spacing $d_g = 1.0a$ for all simulations. Note that the diffusion tensor does not include an iteration superscript (w) because in this formulation the HI depends only on the inter-bead displacements and no preaveraging is used. The diffusion tensor is updated every $\lambda^{RPY} = \Delta t n^{RPY} = 0.05\tau_0$, where $n^{RPY} = 100$ is the the number of time steps between updates.

The conformationally averaged form of the TEA gives the Brownian noise at an accumulated strain ϵ as

$$\tilde{\boldsymbol{\xi}}_i^{(w)}(\tilde{t}, \epsilon) = \tilde{\mathbf{D}}_{ll}^{eff}(\tilde{t}) \langle C_l \rangle^{(w-1)}(\epsilon) \langle \beta' \rangle^{(w-1)}(\epsilon) \sum_{m=1}^{3N} \frac{\tilde{\mathbf{D}}_{lm}^{eff}(\tilde{t})}{\tilde{\mathbf{D}}_{ll}^{eff}(\tilde{t})} f_m(\tilde{\mathbf{t}}) \quad (8)$$

Note the index l gives an individual component of the size $3N$ noise vector and not three components (x, y, z) for a

bead i as in Eqn. 6. The TEA is a pairwise approximation to the exact decomposition. The β' parameter describes the average hydrodynamic coupling and the coefficients C_l ensure the beads experience the correct Stokes drag. The average quantities sampled from the previous iteration are evaluated transiently to account for startup and relaxation transience, leading to

$$\langle \beta' \rangle^{(w)}(\epsilon_o) = \frac{1}{T} \sum_{\epsilon_o t \in \epsilon_{bin}}^{(\epsilon_o+1)t \in \epsilon_{bin}} \beta'^{(w)}(t) \quad (9)$$

$$\langle C_l \rangle^{(w)}(\epsilon_o) = \frac{1}{T} \sum_{\epsilon_o t \in \epsilon_{bin}}^{(\epsilon_o+1)t \in \epsilon_{bin}} C_l^{(w)}(t) \quad (10)$$

where ϵ_o refers to the strain bin, and the sums indicate sampling of a strain interval during the stretching phase and a time interval during the relaxation phase as detailed in the authors' previous work.³⁸ The instantaneous samples of the average are defined as

$$\beta' = \frac{1 - \sqrt{1 - 3N(\epsilon^2 - \epsilon)}}{3N(\epsilon^2 - \epsilon)} \quad (11)$$

where ϵ is an average over the off-diagonal entries of the diffusion tensor

$$\epsilon = \frac{1}{(3N)^2} \sum_l \sum_{m \neq l} \frac{\tilde{\mathbf{D}}_{lm}}{\tilde{\mathbf{D}}_{ll}} \quad (12)$$

The coefficients are given by

$$C_l = \sqrt{\frac{1}{1 + \beta'^2 \sum_l \sum_{m \neq l} \frac{\tilde{\mathbf{D}}_{lm}^2}{\tilde{\mathbf{D}}_{ll} \tilde{\mathbf{D}}_{mm}}} } \quad (13)$$

Further details are given by Geyer and Winter⁶⁴ and the authors' previous work.³⁸ We make minor modifications to the method for the blend case. In principle, there are coefficients C_l associated with each bead. Assuming polymers to be distinguishable only by their initial configurations, we previously used an ensemble averaged set of $3N_L$ coefficients for each linear chain. For blends, there is an additional set of $3N_R$ coefficients for rings. The β'

parameter is a solution averaged quantity that is not specific to the chain architecture. We perform two iterations to obtain freely draining (FD, $w = 0$) and hydrodynamically interacting (HI, $w = 1$) results. The authors have shown that the second iteration ($w = 1$) provides excellent agreement with traditional BD simulations, and a third ($w = 2$) iteration does not significantly improve accuracy.³⁸

C. Experimental Methodology

To prepare ring-linear polymer blend solutions with trace molecules, small amounts of 45 kbp circular DNA molecules are first fluorescently labeled with an intercalating dye (YOYO-1, Molecular Probes, Thermo Fisher) with a dye-to-base pair ratio of 1:4 for >1 h in dark at room temperature. Trace amounts of fluorescently labeled 45 kbp DNA are then added to background solutions of unlabeled 45 kbp semidilute ring-linear DNA blends. Details regarding the preparation of 45 kbp circular DNA and semidilute ring-linear DNA blend solutions are described elsewhere.^{20,34}

Single molecule fluorescence microscopy and imaging is performed using an inverted epifluorescence microscope (IX71, Olympus) coupled to an electron-multiplying charge coupled device (EMCCD) camera (iXon, Andor Technology) as described in detail before.^{32,65} In brief, labeled DNA blend solutions are introduced into a PDMS-based microfluidic cross-slot with 300 μm in width and 100 μm in height. A 50 mW 488 nm laser directed through a 2.2 absorbance neutral density (N.D.) filter (Thorlabs, NJ, USA) is reflected by a 488 nm single edge dichroic mirror (ZT488rdc, Chroma) and used to illuminate the labeled DNA molecules. Fluorescence emission is collected by a 1.45 NA, 100 \times oil immersion objective lens (UPlanSApo, Olympus) followed by a 1.6 \times tube lens and a 525 nm single-band bandpass filter (FF03-525/50-25, Semrock) in the detection path. Fluorescence images are acquired by an Andor iXon EMCCD camera (512 \times 512 pixels, 16 μm pixel size) under frame transfer mode at a frame rate of 33 Hz (0.030 s⁻¹).

III. RESULTS

To investigate polymer dynamics, we primarily consider the fractional extension in the flow direction, $\Delta x/L$. In simulation, the extension is $\Delta x = \max(x_i) - \min(x_i)$. For linear polymers, the contour length is $L_L = (N_L - 1)r_{max}$, whereas for ring polymers $L_R = (N_R - 1)r_{max}/2$ due to the closed loop constraint. In experiment, the extension can be directly visualized and normalized by the ring contour length $L_R = 10\mu\text{m}$.

We also probe the solution rheology via the reduced extensional viscosity, in which we have normalized by the monomer concentration to account for the linear concentration dependence and used c^* as the reference concen-

tration

$$\eta_r = \frac{\eta_p c^*}{\eta_s c} \quad (14)$$

where η_p is the polymer contribution to the extensional viscosity

$$\eta_p = -\frac{\tau_{p,xx} - \tau_{p,yy}}{\dot{\epsilon}} \quad (15)$$

and $\tau_{p,\alpha\beta}$ is the polymer contribution to the stress tensor determined by the Kirkwood formula⁶

$$\tau_{p,\alpha\beta} = \frac{1}{V} \sum_i^N \sum_{j>i}^N r_{ij,\alpha} F_{ij,\beta} \quad (16)$$

$F_{ij,\beta}$ is the conservative force between particles i and j in the β direction.

A. Comparison between simulation and experiment

While simulation variables are matched to experimental conditions as possible, there are limitations which prevent quantitative comparison. First, we use a flexible chain with a FENE-WCA force law, as compared to the wormlike force-extension behavior of DNA. Polymer stiffness influences the extensional rheology of polymer solutions,⁶⁶ suggesting differences in conformational dynamics. The FENE-WCA force law was used for convenient implementation of topological constraints on the length scale of an individual Kuhn segment. Generally, WLC models used in simulation are coarse-grained,⁶⁷ which is not sufficient for capturing hooking behavior. WLC models on the level of an individual Kuhn segment have been developed,^{68,69} but they are incompatible with steep LJ excluded volume potentials without the use of a predictor-corrector integrator, which are computationally inefficient in semidilute solutions. Thus, alternative algorithms for preventing spring crossings such as spring-spring repulsions⁷⁰ or slip-links⁷¹⁻⁷³ would be required. Implementation in a semidilute solution of fine-grained polymers is non-trivial, however. It is also not clear if these approaches developed for coarse-grained models would be accurate in the current study.

Second, simulations consider relatively short chains with $n_K \approx 83$ Kuhn segments per chain as compared to $n_K \approx 200$ for 45 kbp ring DNA and λ -DNA (48.5 kbp). Simulations are limited to short chains because of the size of the box, with the current $N_R = 150$ systems using $N = 19,200$. Higher molecular weight chains would require larger systems, which are intractable due to the $O(N^2)$ computational scaling of the CA method. BD algorithms with improved computational scalings of $O(N)$ ⁷⁴ or $O(N \log N)$ ^{75,76} may help in overcoming this limitation, although they have not been implemented in the CA method.

Third, there are differences in the implementation of flow. Simulations consider a periodic domain in unbounded homogeneous planar extension. While we set the simulation cell size to limit artificial self-interactions of the chain, it is challenging to eliminate these effects because HI are long-ranged. Experiments are performed in a $300 \times 300 \times 100 \mu\text{m}$ cross-slot, and the accumulated strain at the stagnation point is $\epsilon_H \approx 7 - 10$. While the trapped ring is exposed to high strain, the boundary conditions of the cross-slot require continuous inflow of background solution. As we show in Sec. IV, the accumulated strain of the background polymers is important to threading dynamics. In contrast, all chains in are exposed to the same applied flow in simulation.

Finally, while the applied flow is planar extensional in both simulations and experiment, it is not clear the resulting flow with polymers is the same. In simulation, we observe modification of the solvent velocity due to the polymer disturbance. Flow measurements with simultaneous polymer trapping are challenging in experiment, so direct comparison is not made in this work. However, previous work has shown global asymmetric unsteady flow which is sensitive to channel shape,^{45,47,48} channel aspect ratio,⁷⁷ polymer concentration and molecular weight.^{47,78} These observations are directly connected to the geometry of the cross-slot, and thus there may be qualitative differences compared to the unbounded flow implemented in molecular simulation.

B. Relaxation after flow cessation

The longest polymer relaxation time is determined by fitting a single exponential to the linear entropic regime¹⁹ $\Delta x/L < 0.3$ after cessation of constant strain rate flow following an applied strain $\epsilon = 20$. Fig 1 shows the ensemble average relaxation for varying blend ratio. In all cases we find a good fit to $\Delta x = (\Delta x_0^2 - \Delta x_\infty^2)\exp(-t/\tau_R) + \Delta x_\infty^2$. The resulting τ_R normalized by the dilute limit ring relaxation time $\tau_{R,d}$ is plotted versus blend ratio in the inset and compared to results from single molecule experiments. We find the relaxation time decreases weakly with blend fraction of rings f_R . Simulations agree with experiments to within the stochastic distribution of single molecule relaxation times.

We fit the linear polymer relaxation trajectories in the same way and find a similar dependence on blend fraction. Generally, we find that at the same molecular weight, the linear polymer relaxation time τ_L is larger than τ_R ($\tau_L \approx 3.5\tau_R$) because rings are topologically constrained such that they cannot satisfy the lowest order Rouse mode boundary condition.²⁴ We primarily refer to the Weissenberg number as defined using the ring polymer relaxation time Wi_R to describe ring dynamics. However, when considering the solution average flow properties of blends, there are a spectrum of relaxation modes associated with the two components. Thus, we also report the linear polymer relaxation time when ap-

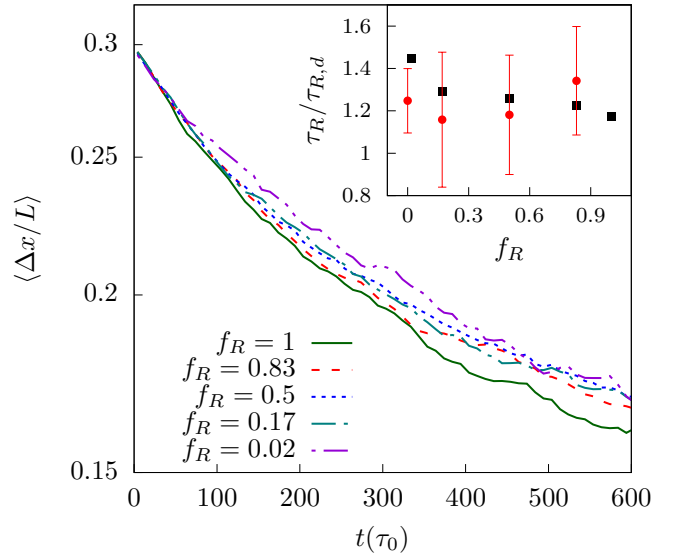


FIG. 1. Ensemble average fractional extension $\Delta\langle x/L \rangle$ relaxation from stretched steady state conformations at $Wi_R \approx 1.5$ after flow cessation for decreasing blend fraction of rings $f_R = 1$ (green solid line), $f_R = 0.83$ (dashed red line), $f_R = 0.5$ (dotted blue line), $f_R = 0.17$ (dash dot teal line), and $f_R = 0.02$ (dot dash violet line). Inset: Ring polymer relaxation time at c^* normalized by the dilute limit value as a function blend ratio from simulation (black squares) and experiment (red circles).

propriate, such as in the solution flow modification for a trace ring in a semidilute linear background (Sec. IV B 4). It may be useful to determine a nominal relaxation time from the decay of solution average properties including the extensional viscosity and the birefringence, but in this study we consider only the polymer conformational relaxation time.

C. Transient molecular conformations

Next we investigate the transient conformations of ring polymers in startup and steady state planar extensional flow. In Fig. 2 we present BD simulation results at a fixed strain rate and decreasing blend fraction of rings $f_R = 0.02 - 1.00$. The ring polymer Weissenberg number $Wi_R \approx 1.5$ is approximately constant, with slight variations because the ring polymer relaxation time decreases with ring blend fraction.

For a pure ring solution, polymers stretch in the flow direction and then exhibit small fluctuations around the steady state average. The ensemble average extension reaches a constant at $\epsilon \approx 4 - 5$. This steady state is achieved faster than in the case of dilute or semidilute linear polymer solutions, consistent with previous experiments and simulations of dilute ring polymer solutions.^{23,24} The faster stretching of ring polymers was ascribed to reduced molecular individualism among

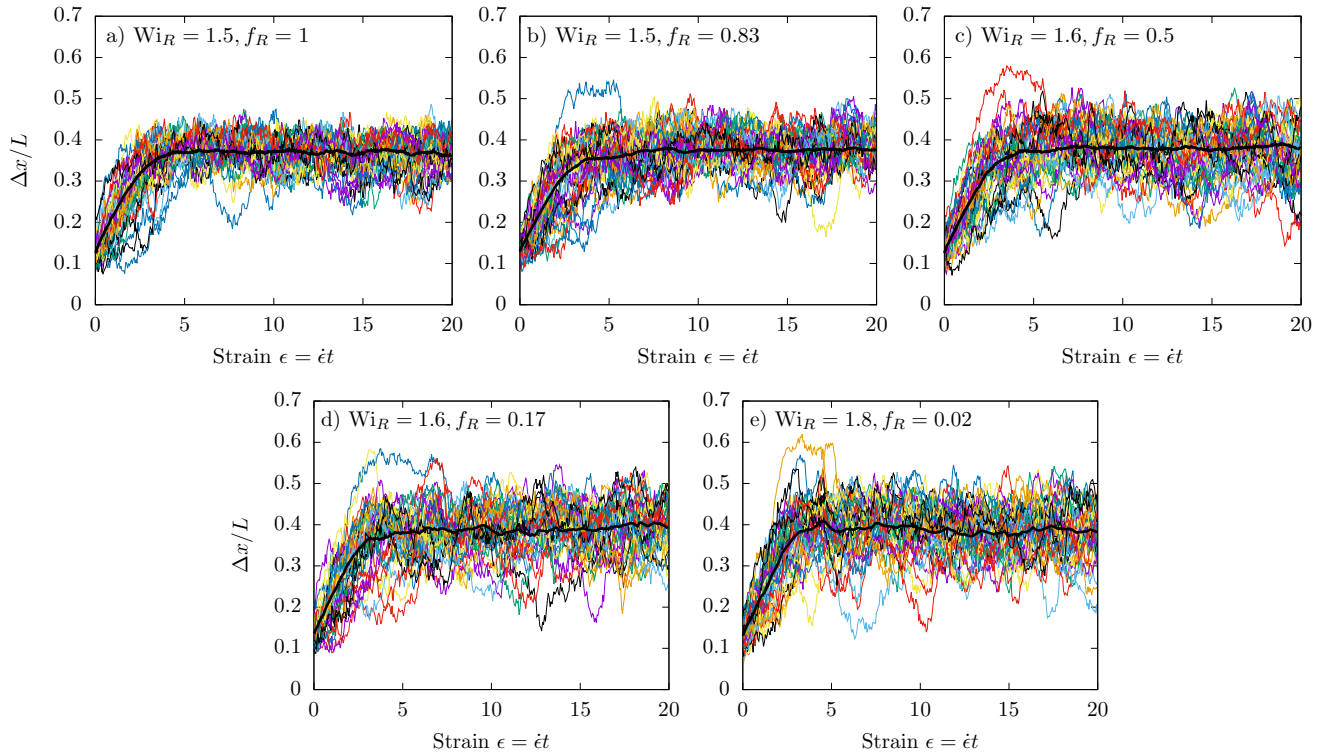


FIG. 2. BD simulation results for individual (colored) and ensemble averaged (black) molecular trajectories of ring polymer fractional extension $\Delta x/L$ vs accumulated Hencky strain ϵ with decreasing ring polymer fraction of a) $f_R = 1$, b) $f_R = 0.83$, c) $f_R = 0.5$, d) $f_R = 0.17$ and e) $f_R = 0.02$ at a fixed flow strength of $Wi_R \approx 1.5$. Only 40 trajectories of the 100-200 molecule ensembles are shown for visual comparison with experiments. Rings in blend with linear polymers ($f_R < 1$) exhibit overshoots in extension on startup of flow and large fluctuations at steady state.

rings. Once steady state is reached, the dynamics are consistent with previous semidilute linear polymer solution simulations.³⁸

For blends of ring and linear polymers, however, we find markedly different behavior. While the ensemble average fractional still plateaus at $\epsilon \approx 4 - 5$, a subpopulation of rings stretches significantly beyond the average to $\Delta x/L \approx 0.5 - 0.6$. This behavior is most noticeable upon the startup of flow, although for majority linear polymer blends, rings can also reach highly stretched conformations $\Delta x/L > 0.5$ at steady state. Additionally, after the steady state average extension is reached, rings can retract back to equilibrium levels of extension $\Delta x/L \approx 0.1 - 0.2$. These conformations are not steady. The extension of individual rings fluctuates significantly in time, consistent with the authors' previous³⁴ and current experiments. Most rings fluctuate in the range of $\Delta x/L \approx 0.3 - 0.5$. These fluctuations grow in magnitude as the blend fraction of rings decreases, which we quantify in the following section.

We also present results from experiments at similar conditions in Fig. 3, where $Wi_R \approx 1.5$ and $f_R = 0.00 - 0.83$. The majority ring polymer solution $f_R = 0.83$ is consistent with the $f_R = 1$ simulation results. Rings stretch to the steady state average and exhibit small

fluctuations. As the blend fraction of rings decreases, large fluctuations emerge as seen in simulation. While the trends are comparable there are noticeable quantitative differences, which we ascribe to the inconsistencies between simulation and experiment discussed in Section III A. Despite these discrepancies, we find that the qualitative agreement is sufficient that the detailed molecular information available from simulation is valuable in understanding the dynamics and rheology of ring-linear polymer blends.

D. Average conformational fluctuations

We quantify the conformational fluctuations described above via the 'steady state' ensemble average fluctuation quantity

$$\langle \delta \rangle = \frac{\sum_{i=1}^n \sum_{\epsilon_{ss}}^{\epsilon_{cess}} \sqrt{(x_i(t)/L - \langle x_i/L \rangle)^2}}{n(\epsilon_{cess} - \epsilon_{ss})} \quad (17)$$

where n is the ensemble size, ϵ_{ss} is the accumulated strain at which the ensemble average fractional extension plateaus, and ϵ_{cess} corresponds to flow cessation. We thereby remove effects of initial transient stretching, although ring polymers in solution blend with linear chains

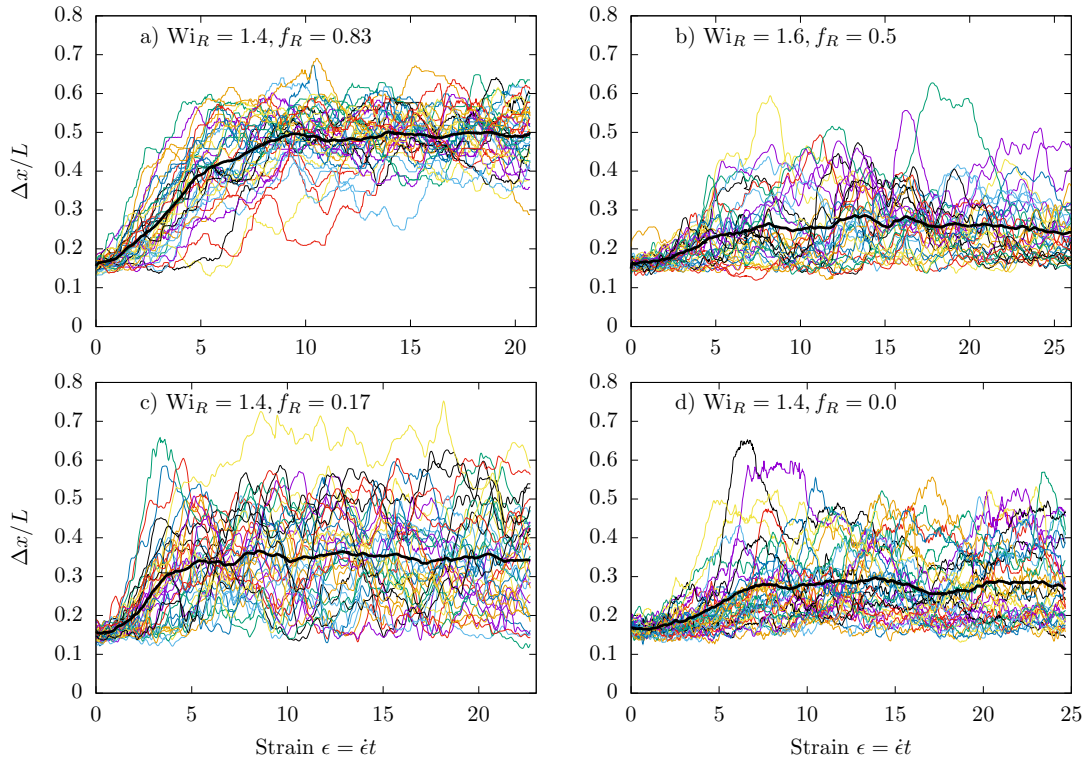


FIG. 3. Single molecule experiment results for individual (colored) and ensemble averaged (black) molecular trajectories of ring polymer fractional extension $\Delta x/L$ vs accumulated Hencky strain ϵ with decreasing ring polymer fraction of a) $f_R = 0.83$, b) $f_R = 0.5$, c) $f_R = 0.17$ and d) $f_R = 0.0$ at a fixed flow strength $Wi_R \approx 1.5$. Experiments exhibit qualitative agreement with simulations in extension overshoots on startup of flow and fluctuations at steady state.

never reach true steady state conformations. This definition is consistent for both ring and linear polymers, with the linear steady state strain $\epsilon_{ss} \approx 8 - 9$, as compared to $\epsilon_{ss} \approx 4 - 5$ for the rings.

In Fig. 4, we report the fluctuation quantity as a function of Wi for a variety of architectures and blend ratios as determined from simulation and experiment. In all cases, the dimensionless flow rate Wi is determined using the relaxation time upon cessation of planar extensional flow at the relevant concentration and blend ratio. In addition to the simulations and experiments presented in this work, we have included results for the case of a pure linear solution at $1 c^*$ and a dilute ring polymer solution from previous work.^{35,38}

In simulation, the pure linear solution undergoes a maximum in the fluctuation quantity at $Wi \approx 0.5$, after which $\langle \delta \rangle$ decreases. This is expected because conformational fluctuations are largest at the coil-stretch transition.⁷⁹ For dilute polymer solutions and semidilute solutions performed in the previous work,³⁸ we find consistent behavior with slight quantitative shifts (data not shown). The fluctuation quantity for pure linear solutions determined from experiment is consistently peaked at low Wi , although quantitatively smaller. We again attribute this to the inconsistencies between simulation

and experiment, in addition to the relatively short duration of the experiments³⁵ ($\epsilon_{cess} \approx 5 - 10$) as compared to simulations³⁸ ($\epsilon_{cess} \approx 20 - 30$).

Dilute ring polymer solutions exhibit significantly suppressed conformational fluctuations as compared to pure linear polymer solutions. This is also expected due to the constrained conformations of the ring. In dilute solution, the majority of linear polymer fluctuations arise from end retraction, which are absent in the ring case. This trend appears to be consistent for semidilute pure ring polymer solutions. Fluctuations are larger than the dilute case due to intermolecular HI but are again peaked at low Wi , and both are lower than the linear polymer case. The semidilute ring polymer solution plateaus at high Wi and meets the pure linear solution result.

A distinct departure from the behavior of either pure linear or ring polymer solutions is observed in the case of ring polymers in ring-linear semidilute blends. For all blend ratios presented here, fluctuations are not peaked at $Wi \approx 0.5$. Instead, they increase up to $Wi \approx 1.5$, with a weak decrease thereafter. Furthermore, fluctuations increase as the blend ratio shifts towards linear chains from $f_R \approx 0.83$ to $f_R \approx 0.02$, confirming the visual observations of molecular trajectories in Figs. 2 and 3. Simulation results show that most of this increase occurs

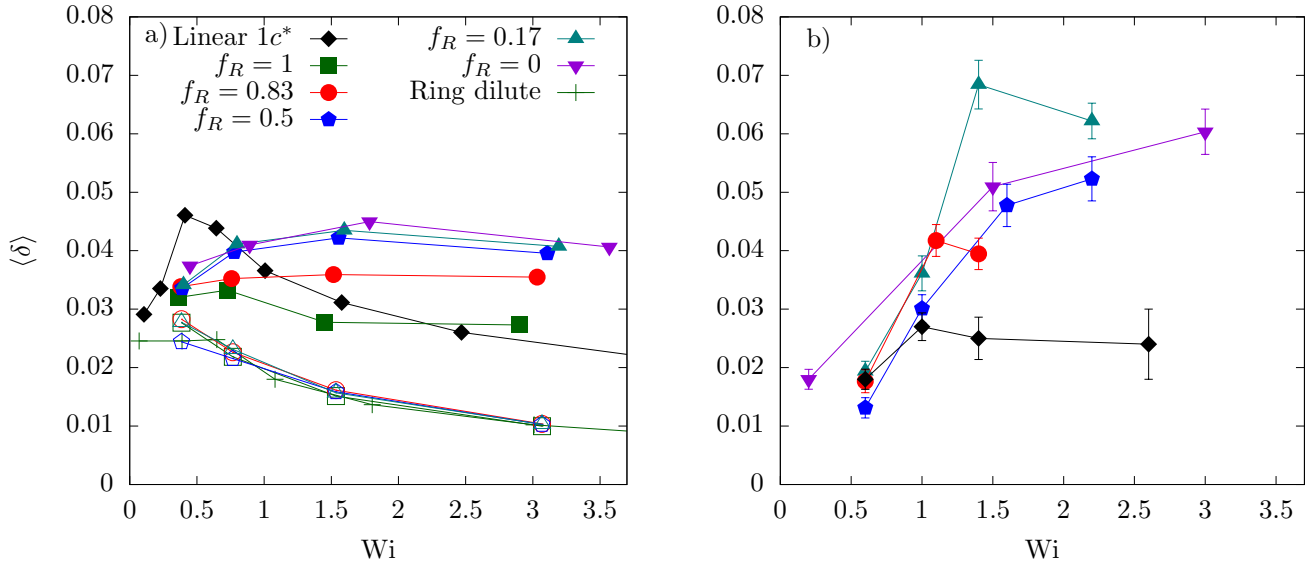


FIG. 4. Ensemble average steady state fluctuation quantity $\langle \delta \rangle$ as a function of Wi for varying blend ratio as determined from a) simulation b) experiment. The Weissenberg number Wi is defined with the appropriate relaxation time for either a ring or linear polymer at the relevant concentration and blend ratio. Closed and open symbols in a) correspond to simulations with and without HI respectively. Conformational fluctuations of ring polymers in blend ($f_R < 1$) increase up to $Wi_R \approx 1.5$, in contrast to pure ring and pure linear solutions, where $\langle \delta \rangle$ is peaked at the coil-stretch transition flow rate $Wi = 0.5$.

from $f_R = 1$ to $f_R = 0.83$, continuing to $f_R = 0.5$. As more linear chains are added, however, further increase in fluctuations are small. This is largely consistent with experiments, which also show increasing $\langle \delta \rangle$ with blend fraction of linear polymers. For $Wi \approx 1.5$, experiments show a non-monotonic trend in fluctuations with blend ratio, with a maximum at $f_R = 0.17$, although this trend is not found in simulations.

To study the influence of HI, we perform ‘freely-draining’ (FD) simulations which neglect HI for semidilute solutions at blend fraction $f_R = 1 - 0.17$. The relaxation time used to define Wi_R , is the Rouse relaxation time. Because the Rouse time is greater than the Zimm relaxation time obtained with HI,^{6,7} the strain rate is reduced to obtain the same values of Wi_R . In the absence of HI, ring fluctuations are significantly suppressed. The semidilute blend results quantitatively agree with the dilute ring solution case, suggesting the FD simulations are effectively non-interacting. This is consistent with previous BD simulations which have shown FD simulations exhibit weak concentration dependence in planar extensional flow.^{37,38}

As compared to the ring polymer component of the blends, the linear polymer component exhibits conformational fluctuations nearly quantitatively consistent with the pure linear semidilute solution case. There is a slight quantitative increase in fluctuations with linear polymer fraction, but the trend is weak compared to the ring polymer case. Thus to the knowledge of the authors, the overshoots in ring extension on startup of flow and the fluctuations at steady state appear unique to rings in semidilute blend with linear polymers. In the remainder

of this section, we investigate other quantities commonly used to describe polymer solution dynamics for further evidence of this feature.

E. Steady state conformations and rheology

The steady state conformations and extensional viscosity of dilute polymer solutions are well understood for linear and ring architectures.^{23,39} Both undergo a transition from an equilibrium coil to a stretched conformation at $Wi \approx 0.5$, although the ring transition is more gradual due to intramolecular hydrodynamics.³⁵ As polymers stretch, the solution viscosity increases due to the entropic restoring force. Given the large instantaneous fluctuations observed for ring polymers in semidilute blends, we are motivated to determine if there is an effect of blend ratio on the ensemble average stretch and bulk viscosity.

In Fig. 5a we plot the ensemble average steady state ring fractional extension after $\epsilon \approx 4 - 5$ versus the blend ratio f_R and Wi_R . We also include results from pure linear solutions at c^* for comparison. The data for the linear component of the blend is not shown because the linear polymer relaxation time is larger than the ring relaxation time, $\tau_L \approx 3.5\tau_R$. Thus the effective linear polymer Weissenberg number $Wi_L = \dot{\epsilon}\tau_L$ at the same strain rate is higher, and the linear chains are stretched for all strain rates presented here. We first observe that the more gradual coil-stretch transition found in dilute solution³⁵ persists in semidilute solution. This is expected because HI

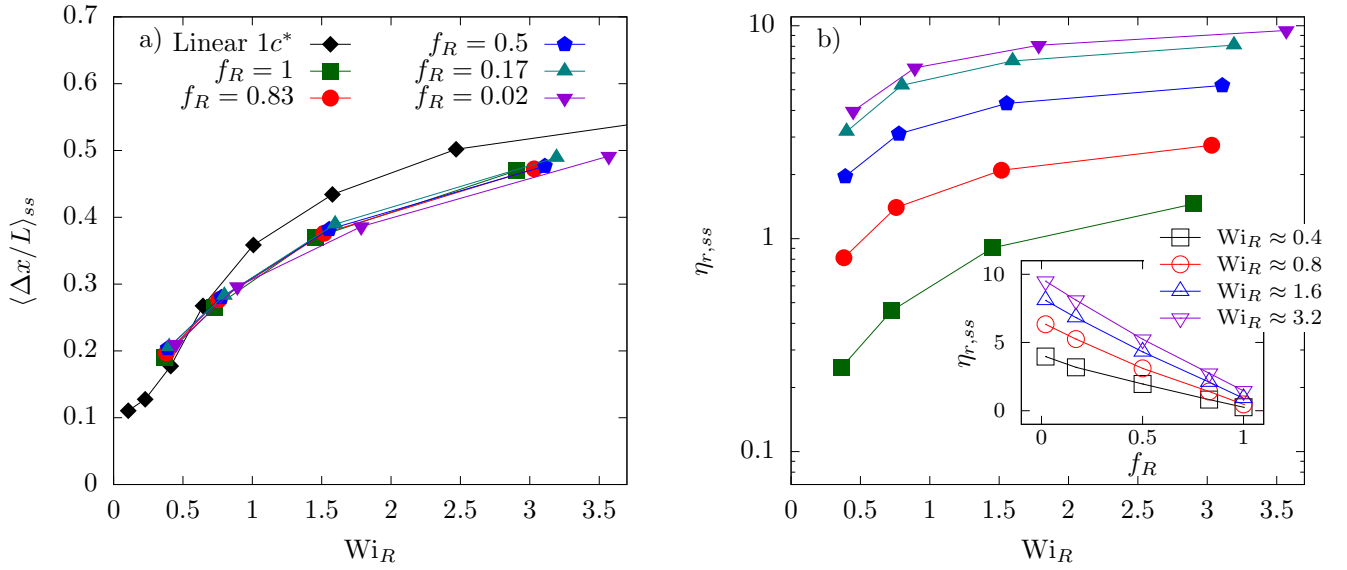


FIG. 5. Ensemble average steady state a) fractional extension $\langle \Delta x/L \rangle_{ss}$ b) reduced extensional viscosity $\eta_{r,ss}$ as a function of Wi_R for varying blend ratio as determined from simulation. Inset: Same data as b) but plotted versus blend ratio f_R at approximately constant Wi_R . Ring polymer extension is nearly independent of blend ratio, but the extensional viscosity decreases with f_R because linear polymers are more stretched than rings. Extensional viscosity varies linearly with blend ratio because the stress is dominated by the linear polymers.

is nominally unscreened at the overlap concentration, and intramolecular HI drives ring extension in the neutral z direction.²⁴ The open ring conformation is significant to both topological interactions and intermolecular HI, as shown in Section IV.

Considering the effect of blend ratio, the average extension curves collapse nearly quantitatively. This suggests that the dominant contribution to the average stretch is only the dimensionless flow strength Wi_R . In the following section we argue this is consistent with the large transient fluctuations. In particular, we show how intermolecular HI and topological interactions can drive instantaneous retraction and extension of the ring polymers.

We consider the influence of blend ratio on steady reduced extensional viscosity $\eta_{r,ss}$ in Fig. 5b. As expected, viscosity increases with decreasing fraction of rings because the stress in unentangled polymer solutions is dominated by stretching. Linear polymers are more stretched than rings at the same strain rate, so as f_R decreases, the linear chain contribution to the polymer stress dominates. When we plot viscosity against f_R at constant strain rate, we find a nearly linear relationship, suggesting the bulk viscosity is determined by simply mixing the linear and ring polymer contributions.

F. Conformational distributions

We conclude our characterization of ring polymer conformations with probably distributions of fractional extension, $P(\Delta x/L)$, in steady and startup flow. Confor-

mational distributions have been widely used to quantify molecular individualism in dilute solution. Currently, we investigate the effect of intermolecular interactions on molecular individualism.

In Fig. 6, we plot the distributions of ring polymer extension for approximately fixed Wi_R and varying blend ratio $f_R = 0.17, 0.83, 1.00$. Results for blend fractions $f_R = 0.02, 0.50$ exhibit near quantitative matching with $f_R = 0.17$ and have been omitted for visual clarity. At low flow rates $Wi_R \approx 0.4$, rings are relatively unperturbed from their equilibrium conformations, and the distribution is nearly quantitatively consistent for varying blend ratio. In the blend cases, the linear chains are moderately stretched to $\Delta x/L \approx 0.4$ because the effective linear flow strength is $Wi_L \approx 1.4$. However, given the small change in ring conformations, it appears that interactions with linear polymers do not affect ring dynamics in weak flow.

When exposed to stronger flows, $Wi_R = 0.8-3.2$, rings are stretched from their equilibrium conformations. Notably, distributions broaden with decreasing fraction of ring polymers f_R for all flow rates $Wi_R > 0.5$. For comparison, we include distributions for linear polymers in a nearly pure linear blend ($f_R = 0.02$) at matched effective flow strength $Wi_R \approx Wi_L$. The comparison clearly shows that the conformational distributions of ring polymers in pure ring solutions agree with those of linear polymers. Specifically, distributions become narrower with increasing flow strength. This is not the case for rings in blend with linear polymers, where distributions are broadest at $Wi_R \approx 1.6$, and broader than the pure polymer solution cases at $Wi_R = 0.8$ and $Wi_R = 3.2$. While the low exten-

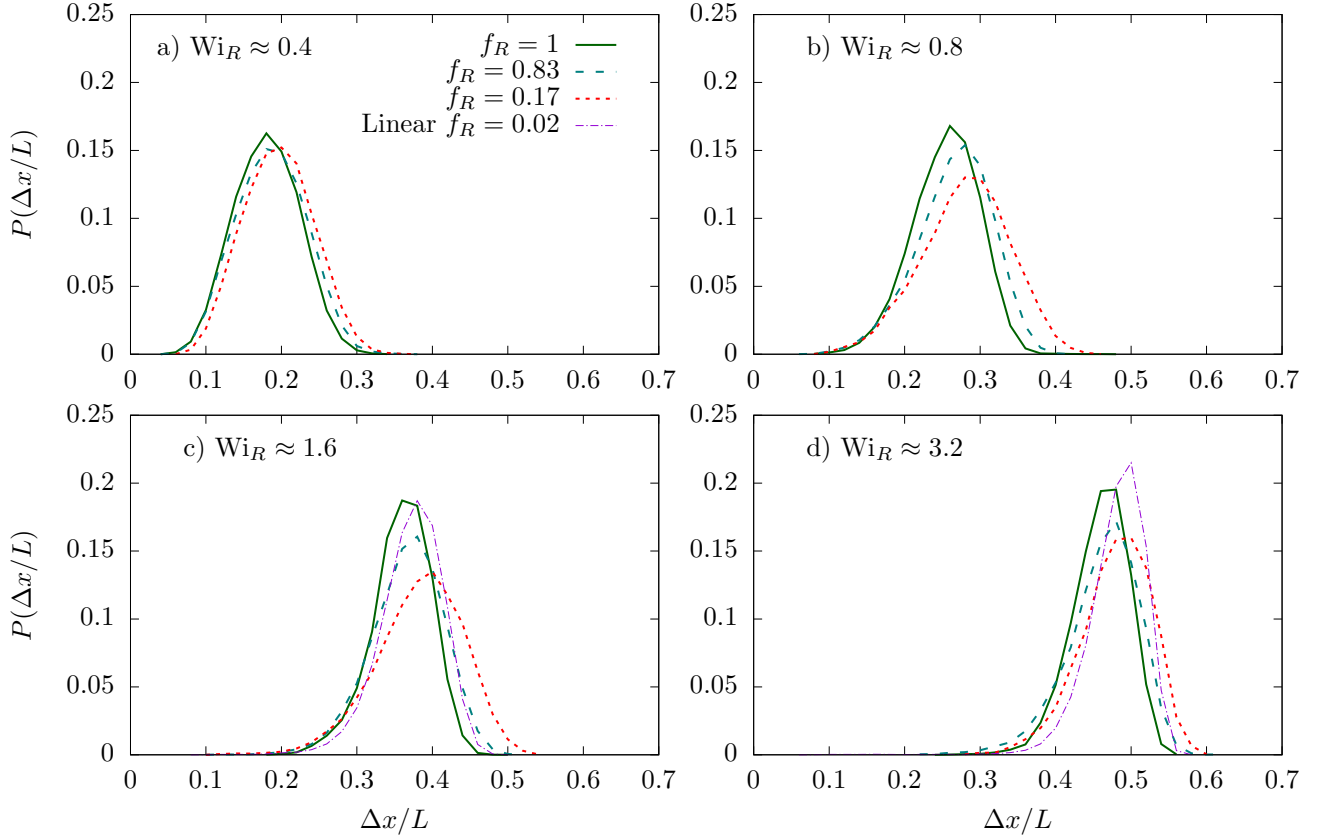


FIG. 6. Steady state distributions of ring polymer fractional extension at blend fractions $f_R = 1$ (solid lines), $f_R = 0.83$ (dashed lines), and $f_R = 0.17$ (dotted lines) for increasing flow rate at a) $Wi_R \approx 0.4$, b) $Wi_R \approx 0.8$, c) $Wi_R \approx 1.6$ and d) $Wi_R \approx 3.2$. For comparison, we include linear polymer distributions (dash-dot lines) in a nearly pure linear polymer solution ($f_R = 0.02$) at similar flow rates with respect to the linear polymer relaxation time at c) $Wi_L \approx 1.4$ and d) $Wi_L \approx 2.7$. Distributions for rings in blend with linear polymers ($f_R < 1$) are broader than for rings in pure solution and linear polymers at all blend ratios.

sion tail is similar for all architectures and blend ratios, ring polymers in blends exhibit a high extension tail that becomes more pronounced with decreasing f_R .

We also quantify molecular individualism upon startup flow transience in Fig. 7. In particular, we consider a constant strain rate $Wi_R \approx 1.6$ and varying blend ratio at increasing accumulated strain from $\epsilon = 2$ to $\epsilon = 6$. We co-plot instantaneous distributions with the steady state averages from Fig. 6, which show transient ring distributions match the steady state conformations after $\epsilon \approx 5$, consistent with the ensemble average extension plateau. First we note features present in all blend ratios; at low strain $\epsilon = 2 - 4$, distributions are broad as some rings have already stretched to the steady state ensemble average extension, while others remain coiled. This is consistent with previous single molecule experiments and simulations, in which the rate of polymer stretching can be divided into subpopulations based on initial conformations. As further strain is accumulated, the distributions narrow towards the steady state case as the majority of polymers become stretched.

Transient distributions of ring-linear polymer blends

are broader than those of pure ring solutions, as in the steady state results. This is apparent even at small blend ratios of linear chains, $f_R = 0.83$. As the blend ratio of rings decreases further, the distribution broadens similar to the steady state case. However, we find another feature in startup of flow at $f_R = 0.17, 0.02$ which is absent at steady state. There is a small population of rings which are highly stretched to $\Delta x/L \approx 0.55 - 0.65$ for $\epsilon = 2 - 5$. In a majority blend of linear chains ($f_R = 0.17$) this effect is nearly negligible, but for a single ring in a linear semidilute background ($f_R = 0.02$), the population is more pronounced. The transient distribution even appears shifted to the right of the steady state at $\epsilon = 4 - 5$, $f_R = 0.02$. In Section IV, we show that this occurs due to hooking of linear polymers with rings.

Overall, conformational distributions are consistent with trends in the average fluctuation quantity $\langle \delta \rangle$ and observations from individual trajectories. Thus, we find a non-trivial dependence of dynamic ring conformations on blend ratio and flow strength despite the collapse of steady ensemble average fractional extension data. In the remainder of this work, we seek to understand these

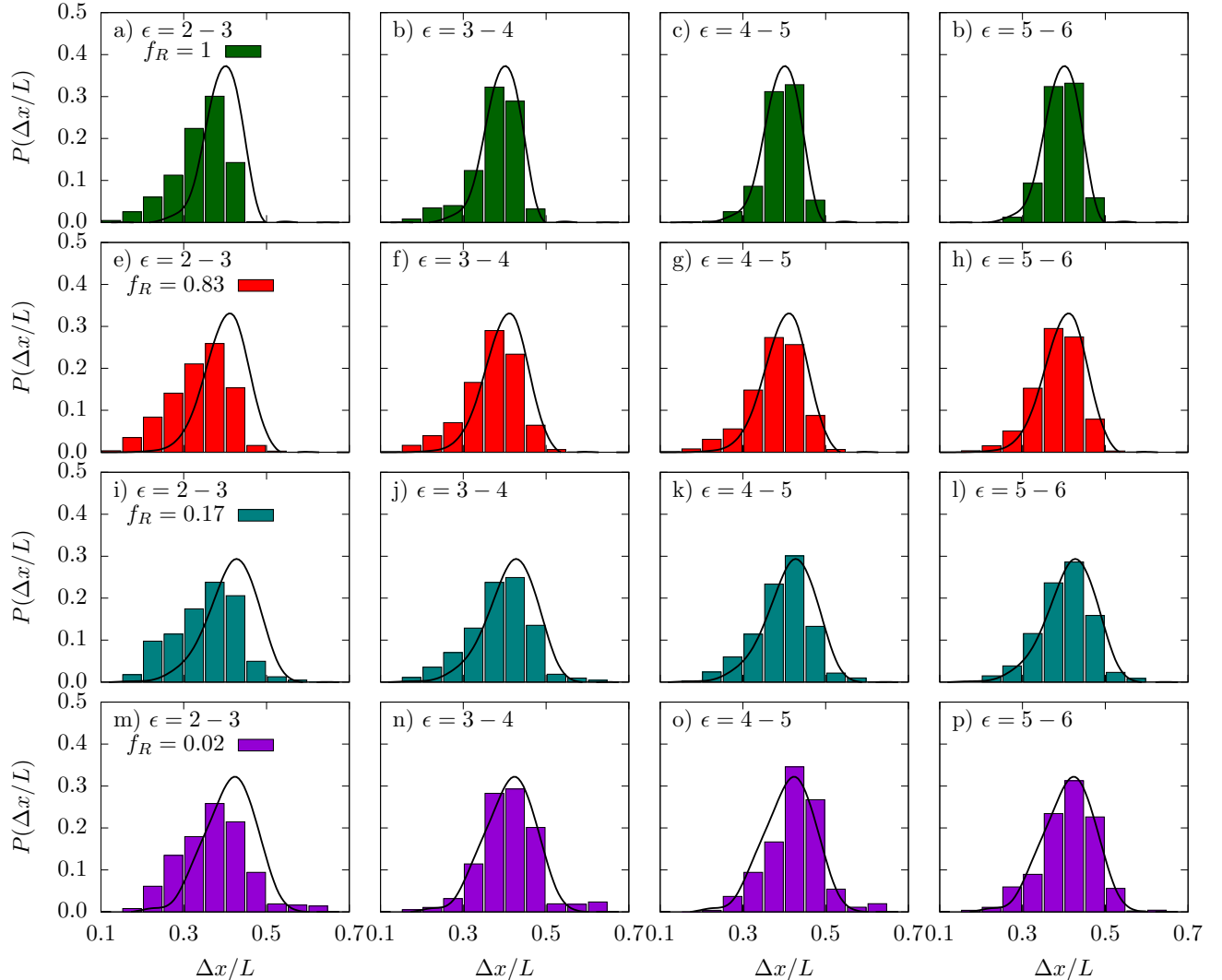


FIG. 7. Transient distributions of ring polymer fractional extension for constant $Wi_R \approx 1.6$, increasing Hencky strain ($\epsilon = 2 - 6$ left to right), and decreasing blend fraction of rings (top to bottom). Blend fractions shown are $f_R = 1$ (a-d), $f_R = 0.83$ (e-h), $f_R = 0.17$ (i-l), and $f_R = 0.02$ (m-p). Rings with a fractional extension $x/L \approx 0.55 - 0.65$ are threaded with linear chains. Steady state distributions are superimposed as lines.

results on the basis of transient intermolecular interactions.

IV. DISCUSSION

We consider two mechanisms for ring conformational fluctuations: i) intermolecular topological constraints in which a ring polymer is ‘hooked’ or ‘threaded’ by a linear polymer or another ring ii) intermolecular hydrodynamic interactions which fluctuate in space and time with the local concentration of linear and ring polymers. As discussed in the introduction, the first mechanism is well motivated by the observation of unique dynamics and rheology in ring polymer solutions and melts from bulk measurements,^{8,14} single molecule experiments,^{30,31} and

molecular simulation.^{13,15} A focus of this work is to determine if flow increases the frequency and importance of ring-linear threading such that the ring dynamics are significantly altered, despite the fact that at equilibrium ring dynamics appear to be unaffected by threading. The second mechanism is motivated by the observation of flow instabilities in low Reynolds number extensional flow of non-dilute polymer solutions. Previous BD-HI simulations have focused on molecular conformations and solution rheology, but we suggest that similar flow modification as observed in experiment and continuum simulations also emerges in molecular simulation. We visualize these flow profiles as a function of time and make direct connections to fluctuations in ring polymer conformations.

A. Intermolecular hooking

We observe three types of topological interactions: ring-linear hooks, ring-ring hooks, and linear-linear hooks. We find ring-linear hooks to be the most common. Linear-linear hooks are less common and thus require a larger ensemble to quantify. We use data from simulation of pure linear polymer solutions at $1c^*$ and $3c^*$ previously published by the authors³⁸ while forgoing the blend cases due to insufficient sampling. Ring-ring hooks are the least common, such that we are unable to quantify their frequency.

1. Observations of ring-linear and ring-ring hooks

We first show simulation snapshots of ring-linear and ring-ring hooks to provide a qualitative description of the conformational dynamics. For examples of linear-linear hooks, we refer to our previous work.³⁸ In the ring-linear case, a polymer is loosely threaded through a ring polymer upon the startup of flow (Fig 8b). At equilibrium, the excluded volume force between the ring and linear polymer is weak due to the low concentration. At low strain $\epsilon = 2.2$, the polymers have not yet collided so the ring stretches at approximately the same rate as the ensemble average (Fig 8c). Upon further strain accumulation, however, the crossing constraint sets in, and the linear chain adopts a folded conformation around the outside loop of the ring, causing it to retract and reorient (Fig 8d). The ring then becomes fully reoriented and overshoots the ensemble average fractional extension before the hook is released and the ring retracts to average levels of extension (Fig 8e,f).

For demonstrative purposes, we have highlighted a trajectory in which the ring both retracts and stretches due to the topological constraint. However, this is a rare occurrence. The majority of ring-linear hooks involve a linear polymer hooked ‘though’ the ring (**Supplementary Information Movie X**) rather than ‘around’, in which case the initial retraction does not occur. Additionally, in this example the linear polymer is already threaded with the ring upon startup of flow. This is the case in the majority of hooks we observe, although it is not required. We include in the Supplemental Information a movie for a trajectory in which an initially unthreaded linear chain adopts a folded conformation, advects into the closed contour of the ring, forms a topological hook that causes an overshoot in ring extension, and then advects away from the ring once the linear chain becomes fully stretched and the constraint is released.

We note that rings tend to hook only with linear chains that adopt ‘folded’ or ‘dumbbell’ conformations.⁸⁰ Linear chains adopting ‘kinked’ or ‘coiled’ conformations lack a hooked structure at their free ends which may advect into the ring. These latter conformations can still thread through the ring, but in this case the excluded volume force is weak because the low polymer concentration al-

lows the ring deform and relax the constraint. Thus, there appears to be aspects of ‘molecular individualism’ as first considered for dilute solution polymer stretching which are relevant in the semidilute case. Due to limited sampling and high computational expense, we are unable to study these problems in further detail here. The influence of Brownian noise is of particular interest for further study, given that we observe ring-linear threaded conformations upon the startup of flow which we would expect to form a strong hook, but do not because the linear polymer stretches before the two polymers collide. This connects to concepts of ‘molecular predestination’, which have been successful in predicting stretching trajectories upon startup of flow on the basis of initial conformations.⁸¹

Next we consider an example of ring-ring hooking. A weakly stretched ring polymer advects towards a stretched ring polymer with position fixed at the stagnation point (dark-orange and light-orange rings respectively in Fig 9b). The unstretched advecting ring then loops around the stretched ring and pulls it towards a coiled conformation (Fig 9c,d). As strain accumulates, the constraint tightens and the ring fixed at the stagnation point adopts a hooked conformation as the advecting ring stretches beyond the ensemble average extension (Fig 9e). Finally, both rings stretch beyond the ensemble average as the constraint is released (Fig 9f), followed by relaxation to average levels of extension in both rings.

As opposed to ring-linear hooks, we find ring-ring hooks form between rings which are initially unthreaded at equilibrium. After the ring ensemble average extension plateaus at $\epsilon \approx 4 - 5$, rings can collide and form strong topological constraints which are not encountered at equilibrium. The excluded volume forces associated with ring-ring hooks are considerably weaker than ring-linear hooks. The tension in the hook is related to the contour length via the flow gradient across the span of the ‘hooking’ polymer. Therefore, at half the contour length of the linear chains, the ‘hooking’ rings impose a weaker constraint and the extra stretching of the ‘hooked’ ring is small. It is not necessary that one of the rings is fixed at the stagnation point, as we show in another example in the Supplemental Information. However, we speculate that in the case of weak topological constraints, fixing the position of one polymer at the stagnation point may increase the frequency of intermolecular hooks.

2. Quantifying hooking behavior

We now establish a procedure for detecting hooks and quantifying how often they occur. For the ring-linear and linear-linear hooks, we detect constraints by a combination of topology strand crossings and excluded volume interactions between hooked chains. In particular, we

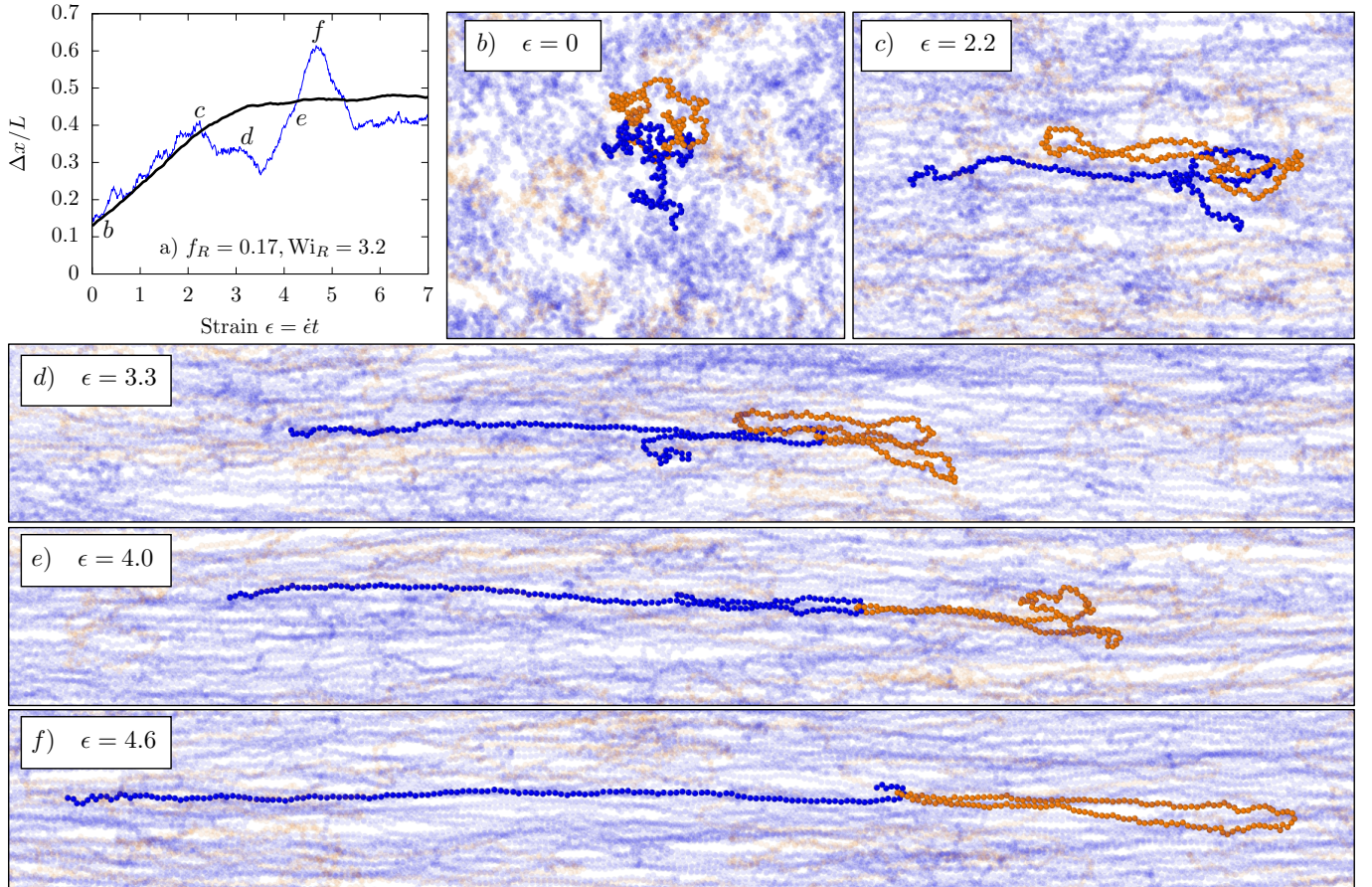


FIG. 8. a) Transient fractional extension for a ring linear polymer which is threaded with a linear chain b) Initially, the linear chain is threaded ‘around’ the outside of the ring c) For low accumulated strain up to $\epsilon \approx 2$, the ring does not feel the constraint and stretches affinely d) the hook inhibits stretching and causes the ring to retract and reorient e) The hook further stretches the ring in until it overshoots the ensemble average and eventually f) the hook is released and the ring returns to the average level of extension.

use the writhe for two polymer chains α and β

$$\begin{aligned}
 Wr_{\alpha\beta} &= \frac{1}{4\pi} \int_{C_\alpha} \int_{C_\beta} d\mathbf{r}_1 \times d\mathbf{r}_2 \cdot \frac{\mathbf{r}_1 - \mathbf{r}_2}{|\mathbf{r}_1 - \mathbf{r}_2|^3} \\
 &\approx \frac{1}{4\pi} \sum_{i=1}^{N_\alpha} \sum_{j=1}^{N_\beta} \frac{\mathbf{r}_i - \mathbf{r}_j}{r_{ij}^3} \cdot (\mathbf{r}_i \times \mathbf{r}_j)
 \end{aligned} \quad (18)$$

where the line integrals are over the continuous polymer curves C_α and C_β are approximated by the discrete bead positions. In the case of a ring, the curve is closed, whereas for a linear chain it is open. While the writhe gives a measure of topological crossings, we are primarily interested in cases where these threads drive changes in the polymer conformation through excluded volume interactions. Thus, we also consider the flow-direction total excluded volume force between the two chains

$$F_{x,\alpha\beta}^{EV} = \sum_{i=1}^{N_\alpha} \sum_{j=1}^{N_\beta} F_{x,ij}^{EV} \quad (19)$$

with the excluded volume force between segments given by Eq. 4. We set a threshold writhe $|Wr_h| = 1$ and excluded volume force $|F_{x,h}^{EV}| = 10kT/a$, which when both are met indicate the presence of a hook. We then determine the writhe and excluded volume force between all chains on a pairwise basis for the simulation trajectories presented in the previous section and assign them a hook status $h_{\alpha\beta}(t)$ as a function of time.

We note that it is challenging to detect ring-ring hooks in this procedure because one half of the penetrating ring will form a positive crossing and the other half a negative crossing, yielding a writhe of zero. Instead, we use only the excluded volume condition for ring-ring hooks and confirm by visual observation. We find ring-ring hooks are nearly negligible at $1 c^*$, in agreement with equilibrium melt simulations showing ring-ring threads are significantly less probable than ring-linear threads.¹⁶ In particular, there are only ~ 10 ring-ring hooks among the 1500 ring trajectories collected at all strain rates and blend fractions $f_R > 0.02$ excluding the trace ring case.

The topological constraint analysis reveals that once

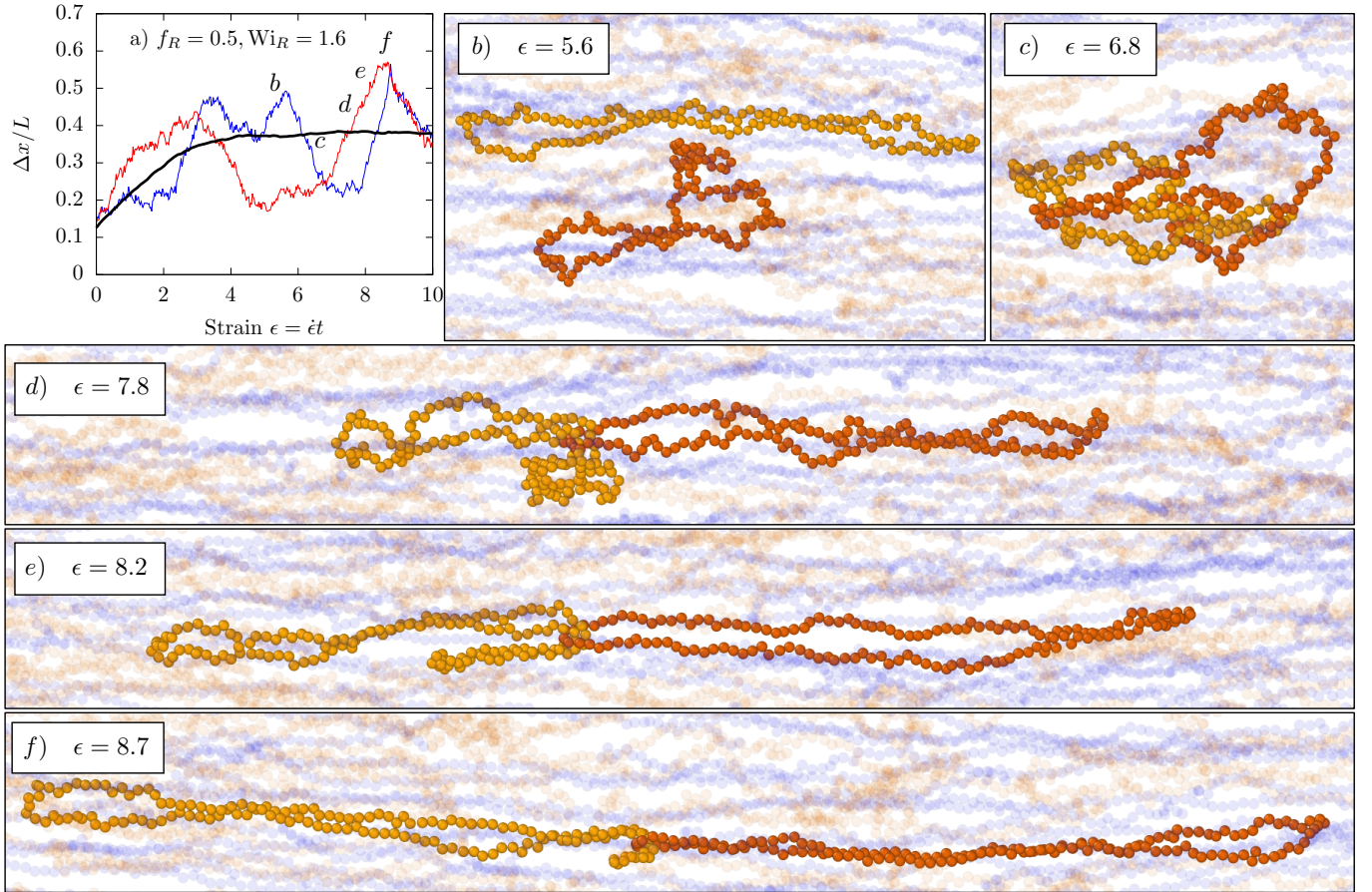


FIG. 9. a) Transient fractional extension for two ring polymers forming an intermolecular hook. The position of one ring is fixed at the stagnation point (blue line, light orange in snapshots), and the other is freely advecting (red line, dark orange in snapshots) b) An incompletely stretched ring polymer approaches the stretched ring fixed at the stagnation point c) The freely advecting ring loops around the fixed ring, causing the fixed ring to recoil d) The pair forms a hook compressing the fixed ring in the flow direction e) The freely advecting ring stretches beyond the ensemble average extension as the hook becomes stronger f) Both rings stretch beyond the average extension due the tension of the hook, followed by constraint release and relaxation.

linear chains are fully stretched, ring-linear hooks are negligible. We explain this by the fact that a linear chain must have a significant end retraction of at least $1/3$ its steady state extension to be able hook with a ring as in the startup flow case. As shown in Fig 4, conformational fluctuations of linear polymers for $Wi_L > 1$ are small due to the large flow gradient across their span. Because of the difference in ring and linear polymer relaxation times ($\tau_L \approx 3.5\tau_R$), the strain rates applied to the blends correspond to $Wi_L = 1.4 - 11.0$. Therefore, we focus on the startup of flow $t = t_0, \epsilon = 0$ to $t = t_{ss}, \epsilon = 8$. In particular, we consider the number of ring-linear hooks per ring polymer, defined as

$$\langle n_h \rangle_{t,n} = \frac{1}{n_{run} n_R (t_{ss} - t_0)} \sum_{i=1}^{n_{run}} \sum_{\alpha=1}^{n_R(i)} \sum_{\beta=1}^{n_L(i)} \sum_{t_0}^{t_{ss}} h_{\alpha\beta}(i, t) \quad (20)$$

where the average is taken over time for the ensemble of ring-linear pairs at a given blend fraction and strain rate. The first summation is taken over the number of

independent simulation runs. This definition accounts for the possibility of multiply-hooked rings, although they are not found in our simulations.

Fig 10 shows the results of the procedure as a function of flow rate and blend fraction. First we note the small quantitative values, reaching a maximum of $\langle n_h \rangle \approx 0.03$ for the case of a single ring in a linear background, indicating that at a given time during startup of flow, only 3% of rings are hooked. Therefore, it appears that topological interactions alone cannot explain the large ring conformational fluctuations observed in simulation. Detailed quantitative study of the transient evolution of hook density and duration remain challenging, although several trends emerge.

A clear result is that the average number of hooks increases with blend fraction. This is expected, as rings form hooks with linear chains more readily than other rings. Majority ring polymer blends $f_R = 0.83, 0.50$ exhibit nearly the same number of ring-linear hooks as linear-linear hooks in a pure linear polymer solution at

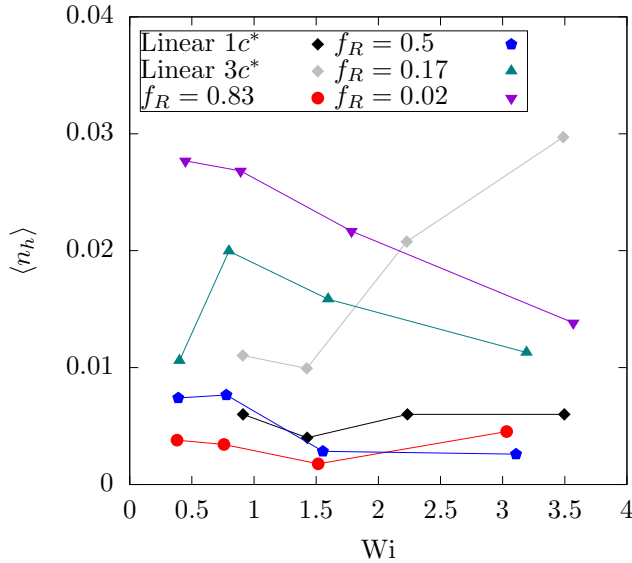


FIG. 10. Time averaged density of ring-linear polymer intermolecular hooks as a function of Wi for varying blend ratio of rings f_R . The density of linear-linear polymer intermolecular hooks in a pure linear solution as determined from previous work by the authors³⁸ is included for comparison. The Weissenberg number Wi is defined with the appropriate relaxation time for either a ring or linear polymer at the relevant concentration and blend ratio.

the same concentration. For majority linear polymer blends $f_R = 0.17, 0.02$, the average number of hooks increases by as much as a factor of 5 at low flow rates. We emphasize that $\langle n_h \rangle$ is determined on a per ring basis, such that blends at lower f_R do not necessarily exhibit a larger number of ring-linear hooks per solution volume.

Another clear trend is the decreasing number of ring-linear hooks for solutions at $1 c^*$ with flow rate. This is in distinct contrast to the pure linear polymer solution at $3 c^*$. We suggest that a crossover in the behavior of topological constraints in strong flows occurs in the range of $c/c^* \approx 1 - 3$. At $1 c^*$, linear polymers threaded through a ring upon startup of flow tend to become fully stretched on a faster time scale than a hook forms for $Wi_R > 2$. Only initial configurations which are ‘predestined’ to hook due to the threading of a folded linear polymer through a ring, for example in Fig 8, form constraints. At lower flow rates, linear chains remain relatively coiled, allowing the constraint time to deform the ring. In the pure linear polymer solution at $3 c^*$, the stretching of polymers to escape the constraint is limited by the surrounding chains. The entanglement concentration for the linear polymer solutions is $c_e \approx 8-10 c^*$, and the equilibrium diffusion follows unentangled scaling at $3 c^*$.⁵⁷ Therefore, our results show diverse behavior as a function of polymer topology, concentration, and flow rate which are not captured by current theories.

We note that Fig 10 does not consider the magnitude of excluded volume force imposed by the constraint or the

resulting chain in ring extension. Further studies with higher molecular weight polymers may reveal the functional effect of ring-linear hooks upon ring conformation and solution stress.

With the current simulation data, quantitative comparison of simulation results to experiments remains challenging. Given that the entanglement concentration is dependent on the polymer molecular weight and flexibility⁷, the higher molecular weight DNA could exhibit more topological constraints than the simulated polymers. Additionally, while the single molecule experiments expose the trapped ring to a total strain of $\epsilon \approx 20 - 25$, the background is continuously flushed with fresh polymer solution that is exposed to a strain of $\epsilon \approx 7 - 10$ before reaching the stagnation point. Previous single molecule experiments and BD simulations have shown that a subpopulation of linear chains can remain coiled to $\epsilon \approx 12 - 15$. Based on our observation that ring-linear hooks involving a stretched linear chain are nearly negligible, this could increase the probability of forming new constraints in the experimental system at steady state. Within the context of molecular simulations utilizing periodic boundary conditions, this case is challenging to reproduce. Fluctuating immersed boundary simulations may be able to reproduce the boundary conditions of the experiment while retaining HI, but the simulation would exceed our computational resources given the the number of polymers and level of fine-grained resolution required.

B. Flow modification by intermolecular hydrodynamic interactions

We now consider the influence of intermolecular hydrodynamic interactions on ring conformational fluctuations. While rings adopt diverse shapes that cannot be completely described by the fractional extension in the flow direction, we observe several characteristic motions we refer to as i) overstretching ii) retraction iii) tank-treading. The first two cases refer to fluctuations in fractional extension more than the three times average fluctuation quantity quantified in Section IIID, $|\Delta x(t)/L - \langle \Delta x/L \rangle| > 3\langle \delta \rangle$, either above or below the steady state average respectively. The third motion refers to rotation of the ring along its contour in the flow-neutral z -direction.

These dynamics are observed at steady state $\epsilon_{ss} > 8$ in the absence of topological constraints. We suggest that the fluctuations can be explained by a modification of the applied flow by intermolecular HI. In particular, we define the total effective flow surrounding a tagged ring polymer as

$$\mathbf{v}^*(\mathbf{r}_i) = \nabla \mathbf{v} \cdot (\mathbf{r}_i - \mathbf{r}_{CoM}) + \sum_j \mathbf{D}(\mathbf{r}_{ij}) \mathbf{F}_j \quad (21)$$

where \mathbf{r}_i is the displacement from the tagged ring cen-

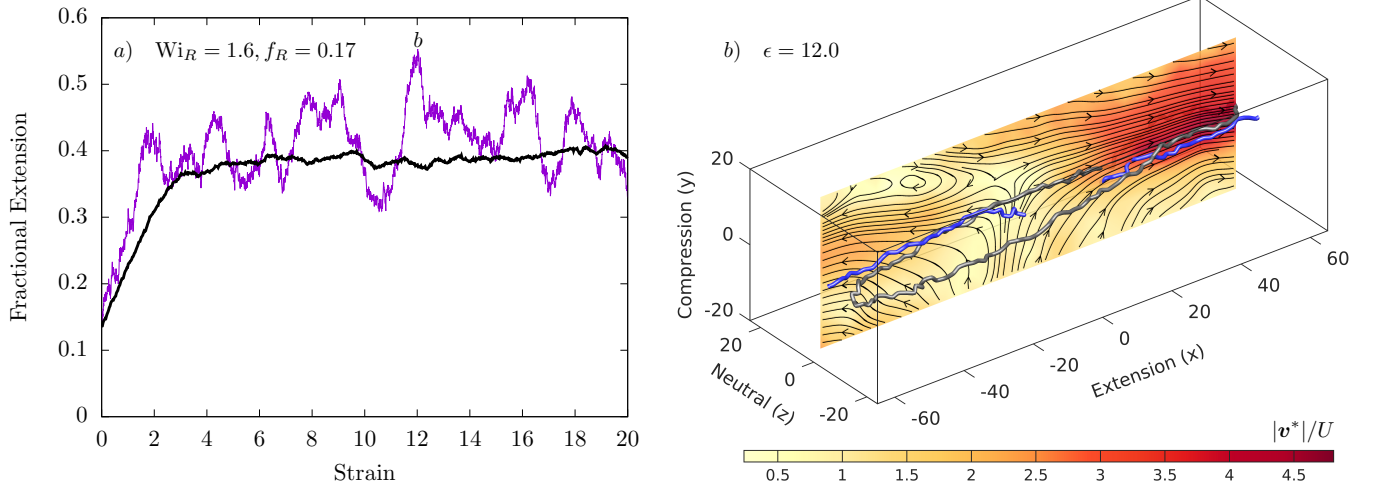


FIG. 11. Ring polymer overstretching a) Transient fractional extension of the tagged ring b) Ring (grey) and linear (blue) polymer conformations superimposed on a slice of the normalized effective flow streamlines \mathbf{v}^*/U in the xy -plane at a location $\tilde{z} = -4$ with respect to the ring center of mass. The snapshot is taken at $\epsilon = 12.0$ corresponding to the maximum in ring polymer stretch. The disturbance velocity of the linear polymers exceeds the underlying applied flow and causes the ring to stretch beyond the steady state average. Other neighboring polymers have been excluded for visual clarity. The ring is slightly stretched in the z -direction such that the strong extension at $\tilde{x} \approx -50$ is not visible in this slice, but the flow is similar to the opposite ‘end’ of the ring at $\tilde{x} \approx 50$. The flow rate is $Wi_R = 1.6$ and the blend fraction is $f_R = 0.83$.

ter of mass \mathbf{r}_{CoM} , $\mathbf{r}_{ij} = \mathbf{r}_j - \mathbf{r}_i$, and \mathbf{r}_j and \mathbf{F}_j are the positions and total conservative force respectively of polymer bead j . The first term accounts for the applied planar extensional flow in the frame of reference of the ring center of mass. Because the applied flow is homogeneous and unbounded, we can define a new origin \mathbf{r}_{CoM} without qualitatively changing the flow measurement to provide a more intuitive flow field. The second term accounts for the polymer disturbance velocity where the sum is over polymer bead indices, and the prime indicates that beads on the tagged ring are excluded. Intramolecular HI, or the ring’s response to the flow, are excluded in order to visualize the forces which drive ring fluctuations. In the retraction case, this is not necessary as the ring is unstretched and the tagged ring contribution to the disturbance is weak. In the overstretching and tank-treading cases, however, the ring can reach highly stretched conformations, yielding strong restoring forces and flow disturbances. The intermolecular HI which drives ring stretching are thus largely cancelled out and not easily visualized when the intramolecular component is included.

The total flow \mathbf{v}^* is then evaluated on a uniform rectilinear mesh grid at locations \mathbf{r}_i surrounding the ring center of mass. We find that snapshots of the flow field on the time scale of a single time step $dt = 5 \times 10^{-4} \tau_0$ are noisy due to Brownian noise. To overcome this, we perform additional simulations which sample the disturbance velocity every 50 time steps for an interval $50\tau_0$ or $0.17\tau_R$. Polymer advection is minimal on this time scale and the resulting streamlines are a close approximation to the instantaneous flow. The flow sampling increases the

computational expense of the simulation by $An_p N$ where A is a constant associated with evaluating the RPY tensor for a grid point polymer bead pair, and n_p is the number of grid points. As n_p exceeds N the simulation becomes computationally expensive, so we consider a volume extending only slightly past the extents of the tagged ring. Visualization of the full 3D flow field is an interesting area for further study but is unnecessary for understanding the dynamics of individual ring polymers.

The effective velocity is normalized by a reference value $U = \max(|\nabla \mathbf{v} \cdot (\mathbf{r}_i - \mathbf{r}_{CoM})|)$ corresponding to the maximum applied flow magnitude on the mesh. For positions further from the ring the applied flow becomes stronger relative to the polymer disturbance, but these flows are not relevant to the ring conformation. We now consider several specific examples of the characteristic motions described above and visualize the surrounding flow fields.

1. Overstretching

In Fig. 11a we show the transient fractional extension of a ring in a majority linear blend $f_R = 0.17$ at $Wi_R = 1.6$ which fluctuates around the ensemble average extension. At $\epsilon \approx 12.0$, the ring becomes highly stretched to $\Delta x(t)/L - \langle \Delta x/L \rangle > 3\delta$. We plot the streamlines for the effective velocity in the xy -plane at this time superimposed with the ring conformation and selected linear conformations in Fig 11b. The effective flow at the ring end $\tilde{x} \approx 50$ is ~ 4.5 times stronger than the applied flow alone, causing the ring to stretch far beyond its average extension. We see that this clearly coincides with the

position of a linear chain end. At the opposite end of the ring, $\tilde{x} \approx -50$ the ring is similarly stretched by a linear chain end, although this is not visible in the displayed slice because the ring is slightly stretched in the z -direction.

Thus, we find that local fluctuations in the polymer concentration drive flow modifications and determine ring conformational dynamics. In particular, the proximity of linear chain ends to ring ‘ends’ can cause overstretching. While the highlighted linear chain ends do not completely reproduce the total flow, they contribute the essential features of strong extension. We note that only a section of the linear chains are shown. The full conformations extend in the flow direction away from the ring. If we approximate the linear chains as dumbbells, the importance of the linear chain ends becomes clear. The stresslet portion of the force dipole leads to a strong disturbance at the chain ends, while the disturbance at the chain center goes to zero.

2. Retraction and tumbling

Next we consider an example of ring retraction at $f_R = 0.5$, $Wi_R = 1.6$. The ring is initially stretched in the flow direction at $\epsilon \approx 13$, at which point a rotational flow field emerges (Fig 12b). The flow causes the ring to retract and undergo ‘end-over-end’ tumbling, passing through a minimum in fractional extension at $\epsilon \approx 15.3$ (Fig 12c). Finally, the flow surrounding the ring returns to approximately planar extension with a stagnation point laterally displaced to $\tilde{x} \approx 40$ (Fig 12d). The ring then completes reorientation in the flow direction and stretches back to average levels of extension. To facilitate visualization of this process, we have colored one half of the ring conformation grey and the other blue, showing that from $\epsilon = 14.3$ to $\epsilon = 16.1$ the two halves essentially exchange places.

Not all cases of ring retraction involve end-over-end tumbling. More often, the ring extension decreases by only $x(t)/L - \langle x/L \rangle \approx 1 - 2\langle \delta \rangle$ before restretching. This is due to the degree of flow modification, with weaker retractions corresponding to a mixed flow between rotation and extension, and end-over-end tumbling corresponding to rotational flow. The molecular mechanism for flow modification in this case is not clear. Both spatial and temporal variations of the flow field are important due to advection of the ring and evolution of the microstructure respectively. We speculate that the rotational flow observed in Fig 12b,c could emerge due to a superposition of rotlet portions of the linear chain force dipoles. Similarly, the mixed flows which drive smaller retractions could be due to a more complex superposition of stresslet fields from linear chains advecting in opposite directions with respect to the extension axis. However, we are not able to identify any minimal set of linear chains which reproduce the total flow as in the overstretching case seen in Fig 11.

3. Neutral direction gradients and tank-treading

In both the overstretching and tumbling cases, we see that the ring is slightly stretched in the z -direction, which is neutral to flow. This is not unexpected, as previous simulations have shown that the coupling of chain architecture and intramolecular HI in rings drives the chain to an open loop conformation.²⁴ The stretching of the ring is the cause of the mild coil-stretch transition and delay in critical Weissenberg number as compared to linear polymers. In the semidilute case, this may be complicated by the screening of HI, which causes rings to compress in the neutral direction as seen in dilute freely draining simulations. Alternatively, the concentration gradients which lead to the mixed flows seen in the extension-compression plane in Figs. 11 and 12 could introduce flow gradients in the neutral direction which are absent in the dilute case.

In Fig 13, we highlight a case where the ring is observed to ‘tank-tread’, meaning the ring rotates along its contour while remaining stretched in the flow direction. We include a simulation movie in the Supporting Information. Tank-treading has been reported for dilute rings in shear flow, where the driving force for rotation is the shear gradient on ring polymers adopting elliptical conformations in the flow-gradient plane.²⁶ Due to the deformability of the chain, tank-treading in rings is not continuous but is coexisting with the end-over-end tumbling motions first observed in linear polymers. For high Wi , clear instances of tank-treading were resolved via an angular autocorrelation function, and a scaling with Wi was found. In this work, the dynamics are markedly different. The applied flow is planar extensional, such that there is no component of rotation and the ring is compressed in the y direction. The tank-treading motion can emerge only due to a combination of intramolecular HI driving the ring open in the neutral direction and intermolecular HI introducing a driving force for rotation.

The origin of rotation is clearly seen in Fig 13a, where the polymer disturbance velocity causes rotational flow in the xz (extension-neutral) plane. We note that the ring does retract slightly during the rotation, as seen in the Supporting Information movie, so the motion is not purely tank-treading. Additionally, we see at a later time, where the ring has rotated around its contour by $\approx 90^\circ$, that the rotational field has returned to primarily extensional flow, although with notable gradients still in the z -direction at the ring ends, $\tilde{x} \approx \pm 40$ (Fig 13b). This evolution of the flow field is directly connected to the motion of neighboring chains. In the simulation movie we highlight three linear polymers which primarily drive the flow. At $\epsilon = 18.1$ (start of the movie), two linear chains which appear overlapping in the extension-compression plane but with a separation in the neutral direction of approximately the ring stretch, $\Delta z_R \approx z_{L1} - z_{L2}$. The linear chains are highly stretched with nearly constant z positions along their contours. The two linear chains are advecting in opposite directions with respect to the

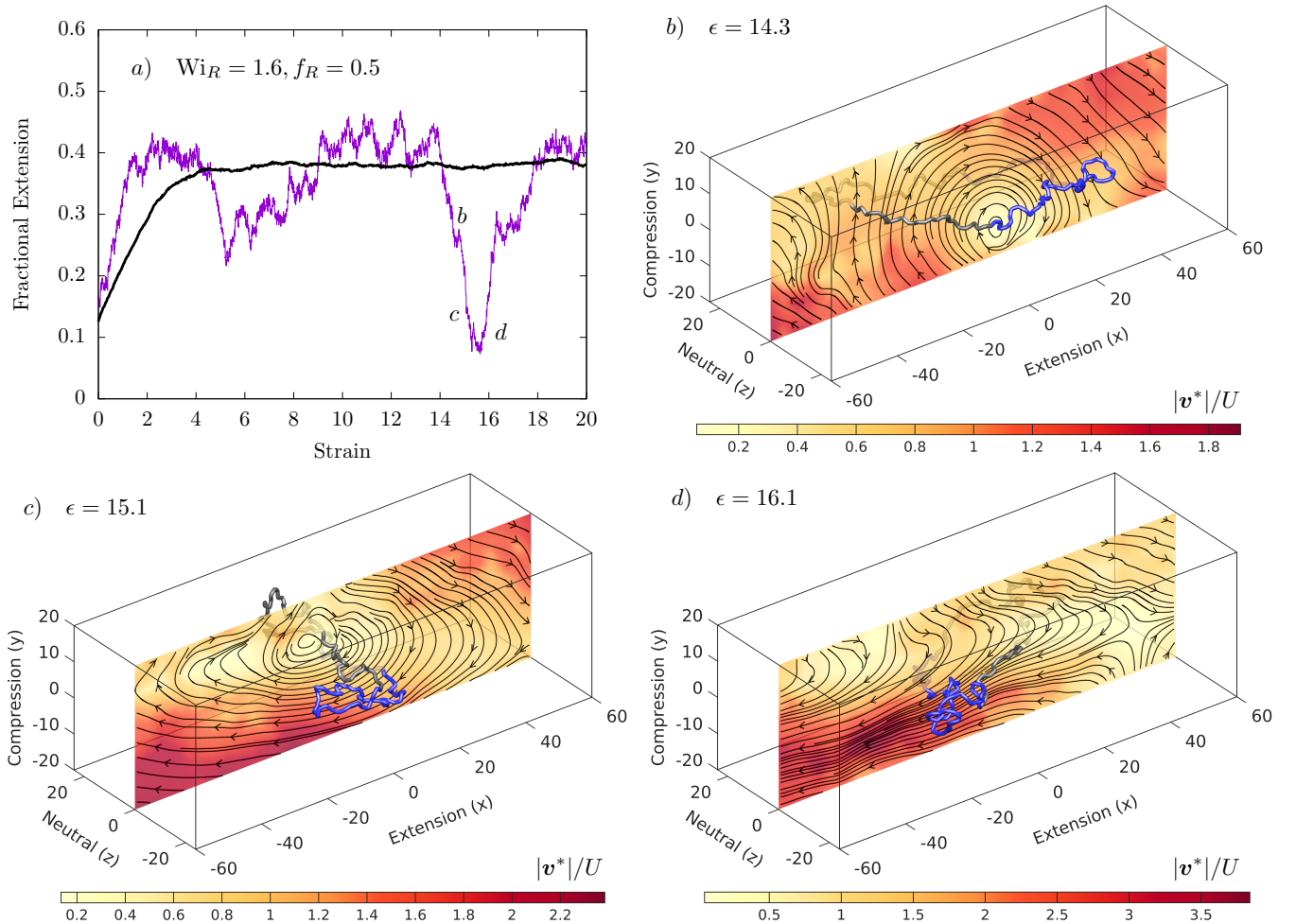


FIG. 12. Ring polymer retraction and tumbling a) Transient fractional extension of the tagged ring b) Ring polymer conformation superimposed on a streamline slice in the xy -plane at $\tilde{z} = 0$ with respect to the ring center of mass. Half of the ring is colored blue and the other half grey to show the ‘end-over-end’ tumbling. The ring is initially stretched in the flow direction before entering the rotational field c) The flow causes the ring to retract and reorient while swelling slightly in the y direction so the ‘ends’ can flow past each other d) The flow returns to approximately planar extension and the ring stretches back to average levels extension after complete reorientation. The flow rate is $Wi_R = 1.6$ and the blend fraction is $f_R = 0.5$.

axis of extension due to their center of mass positions in the applied flow. The superposition of their disturbance velocities leads to the rotational field. Once the linear chains have advected away from the ring, their disturbance decays and the rotational field dissipates, leading to the gradient in the z -direction seen in Fig 13b. A third chain is highlighted which plays a minor role, and other chains which contribute to the total flow are made transparent for visual clarity. Note that at two points during the movie the polymer positions appear to undergo a large instantaneous translation. This is simply an artifact of visualizing the periodic boundary conditions in a deforming simulation box and does not represent the dynamics as they occur in simulation.

More generally, the role of flow gradients in the z direction are challenging to characterize. Tank-treading is rare because the spatiotemporal variations of the flow

occur on time scales shorter than the tank treading frequency. We conclude that the conformational fluctuations as measured in a coarse-grained sense by the average fluctuations in the fractional extension $\langle \delta \rangle$ are due to diverse features of the flow which arise from the polymer disturbance velocity. As the blend fraction of rings f_R decreases, the flow modification increases due to the larger disturbance velocity of the highly stretched linear chains as compared to the lightly stretched rings. However, isolating well defined mechanisms for the dynamics on the basis of intermolecular interactions requires further study. Lower concentration solutions, which have been shown by the authors to exhibit similar fluctuations,³⁴ may be more tractable. A possible direction is to connect local concentration changes to conformational fluctuations. A challenge is that it is not just the concentration but also the direction of the disturbance velocity

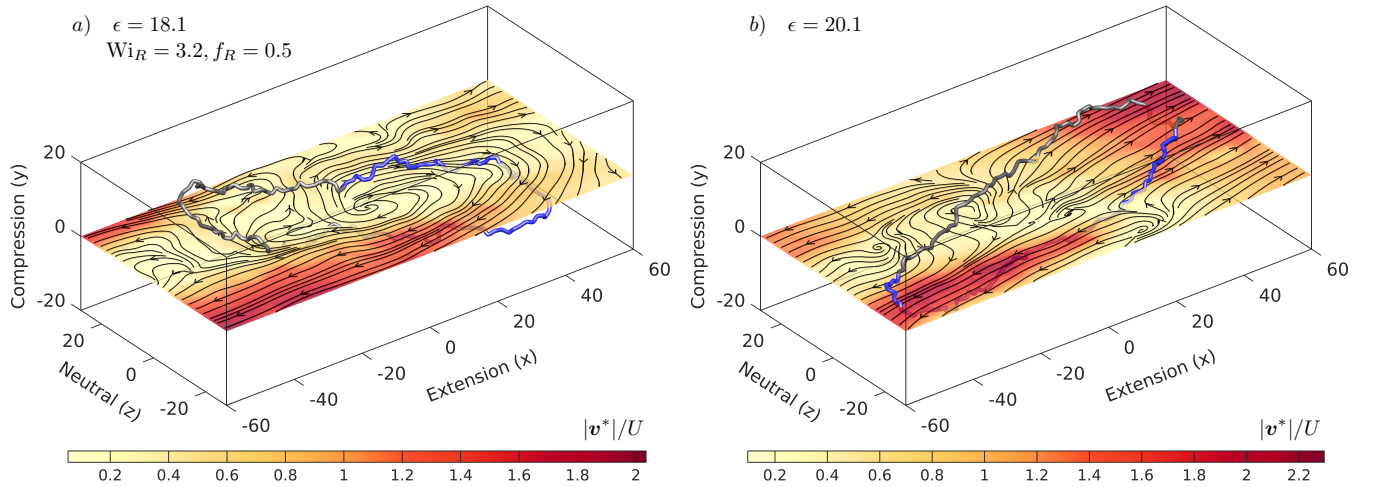


FIG. 13. Ring polymer tank-treading a) Ring polymer conformation superimposed on a streamline slice in the xz -plane at $\tilde{y} = 0$ with respect to the ring center of mass. The ring is initially stretched in an open loop conformation. The flow in the neutral z -direction is rotational, while in the xy -plane it is primarily extensional (not shown), causing the ring to rotate along its contour while remaining stretched in the x -direction b) Upon further strain accumulation, the flow returns to planar extension as the neighboring chains advect, although gradients in the z -direction remain. The flow rate is $Wi_R = 3.2$ and the blend fraction is $f_R = 0.5$.

which determine whether a polymer retracts or stretches. Thus, a model must include the local concentration of polymer segments as well as the orientation of the restoring force on the segments. For example, in a field-based model, the relevant spatial and temporal distribution of segments is $\Psi(\mathbf{r}, t, c, \mathbf{f})$.

4. Bulk flow Modification

Interestingly, we find that many of the flow structures observed in simulation are qualitatively consistent with particle tracking velocimetry measurements of flow in non-dilute polymer solutions in microfluidic devices. In particular, Haward et al. have found transient rotational and shear flows in an optimized-shape cross-slot extensional rheometer (OSCER) for polymer solutions at $c/c^* = 0.1 - 0.4$ and negligible Reynolds number Re .⁴⁷ The authors reported two instabilities in the applied planar extensional flow arising from the extra polymer stress. In particular, they find transient lateral displacement of the stagnation point at moderate $Wi \approx 0.75$ and transient global flow asymmetry at $Wi \approx 2.0$. In this work, we have focused on the flow profile in the Lagrangian frame of a tagged ring. However, if we consider the Eulerian frame we observe the stagnation point displacement (Fig 14a) and transient flow asymmetry instabilities (Fig 14b,c) reported by Haward et al. at consistent Wi values.⁴⁷ There are qualitative differences in simulation because the flow is unbounded. Most notably, the flow asymmetry for $Wi > 2$ decays at distances far from the stagnation point. Additionally, polymers in the OSCER experience finite strain $\epsilon \approx 7$ before flowing out of the hyperbolic region, and the accumulated strain is

dependent on the y position. In simulation, all fluid elements experience the same accumulated strain which in principal is unlimited.

While the resemblance between the flow structures emerging in simulation and experiment is striking, we do not draw further conclusions because of the possibility of finite size effects imposed by using a relatively small periodic simulation box as compared to the polymer size. In the current study, a fine-grained polymer model was required to resolve the influence of topological interactions. Due to this limitation, increasing the system size further is computationally prohibitive and finite size effects cannot be directly investigated. However, if we neglect chain crossing constraints, coarse-grained bead-spring polymer models could be used to access larger length scales. Although originally used in dilute BD simulations, coarse-grained models have also proved useful in predicting detailed features of the solution stress,⁸² and they may also be suitable for investigating the influence of intermolecular interactions on flow instabilities.

C. Test case: a bidisperse linear blend

The observation that ring polymers exhibit large conformational fluctuations due to size and shape differences with the linear portion of the blend raises the question: what is the influence of chain architecture? Is there a unique feature of the ring polymers that causes these dynamics, or is it simply because their contour length is half that of the linear chain? To investigate this topic, we have performed simulations of bidisperse linear polymer solution blends of short $N_S = 75$ and long $N_L = 150$ linear blends. In this case, the contour length of the

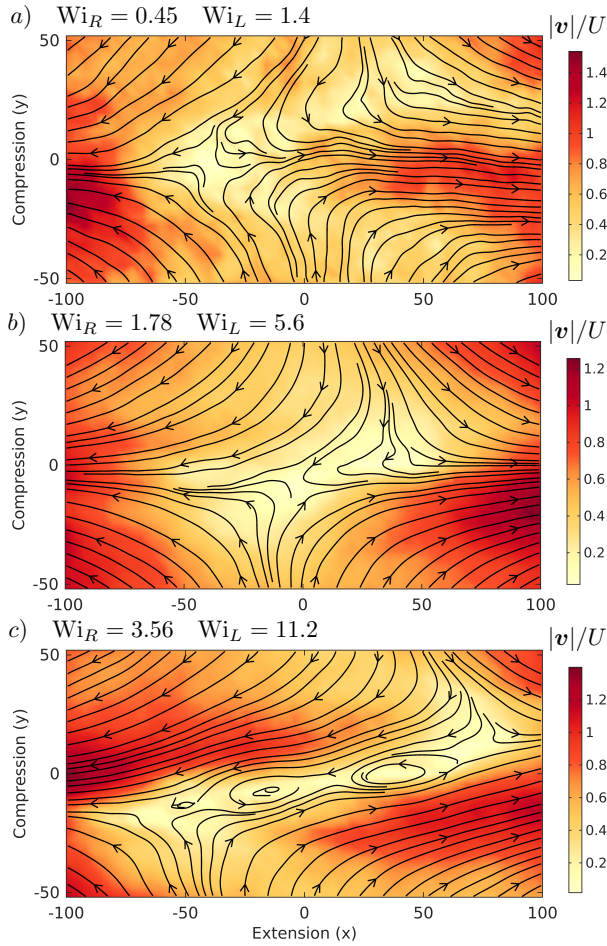


FIG. 14. Total effective flow due to applied PEF and polymer disturbance for a trace ring in a linear semidilute background $f_R = 0.02$ at flow rates a) $Wi_R = 0.5, Wi_L = 1.4$ stagnation point displacement b) $Wi_R = 1.8, Wi_L = 5.6$ transient flow asymmetry c) $Wi_R = 3.6, Wi_L = 11.2$ transient flow asymmetry.

short chains is matched to the rings, $L_S = L_R = 0.5L_L$, and the relaxation time is comparable ($\tau_R = 274\tau_0$ vs $\tau_S = 322\tau_0$ in pure solution $f_R = 1$ and $f_S = 1$ respectively at c_L^*). The polymer concentration by mass $c = N/V$ is matched to the ring-linear blend simulations. We define the mass fraction of short linear chains $f_S = n_S N_S / (n_S N_S + n_L N_L)$, and simulations are performed at $f_S = 1, 0.5$. Essentially, each ring polymer is replaced with two short linear chains, all chains are initialized as non-overlapping random walks, and the TEA parameters are modified appropriately. Otherwise, details of the simulation are the same as described in Section II. We define a Weissenberg for the short linear polymers $Wi_S = \dot{\epsilon}\tau_S$, where τ_S is the short polymer relaxation time at the appropriate blend ratio and is determined by the same procedure as for the ring-linear blends.

In Fig. 15 we compare the results of ring-linear blends and bidisperse linear blends at varying blend fraction and flow rate Wi , where the relaxation time τ_R or τ_S at

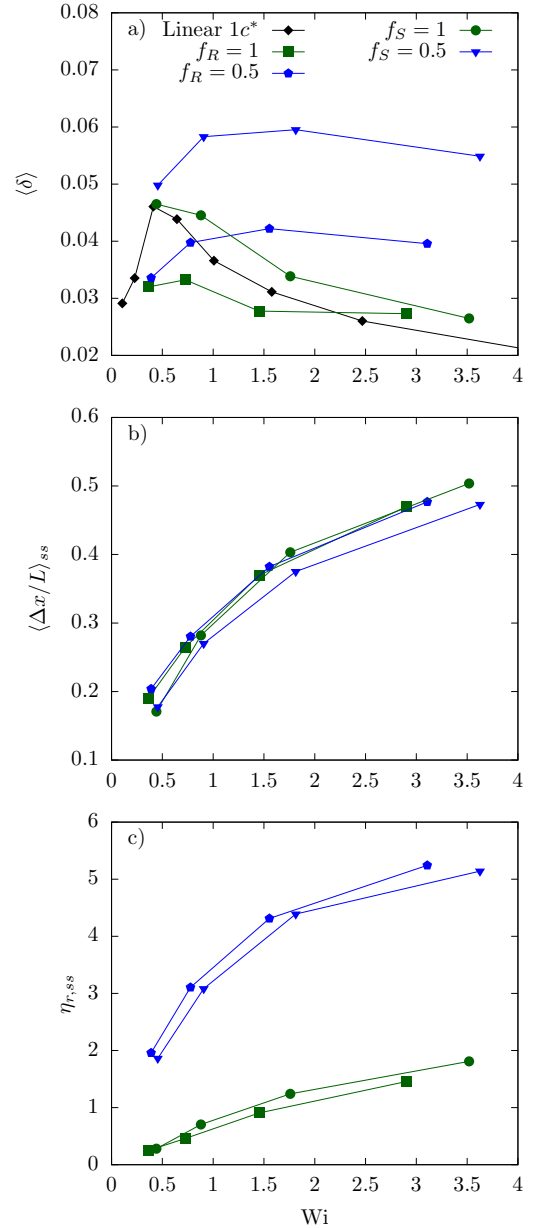


FIG. 15. Ensemble average steady state a) fluctuation quantity $\langle \delta \rangle$ b) fractional extension $\langle \Delta x / L \rangle_{ss}$ c) reduced extensional viscosity $\eta_{r,ss}$ as a function of Wi for ring-linear blends at $f_R = 1, 0.5$ as compared to bidisperse linear blends at $f_S = 1, 0.5$. The Weissenberg number is defined as the strain rate normalized by the corresponding relaxation time for the architecture and blend composition.

the relevant blend fraction is used. The two systems are in qualitative and in some cases quantitative agreement. The primary result is that fluctuation quantity for the short linear chains follows the trend of the rings. In the pure short linear polymer solution $f_S = 1$, $\langle \delta \rangle$ is peaked at $Wi = 0.5$ and monotonically decreases with Wi , in agreement with the reference data.³⁸ In the bidisperse linear blend $f_S = 0.5$, however, the fluctuation quantity

matches the pure solution case at $Wi \approx 0.5$, increases up to $Wi \approx 1.5$, and decreases for stronger flows. We also find that the fluctuations are quantitatively larger than the ring-linear blend case. A clear explanation for this behavior is that at low Wi , the dynamics are weakly dependent on blend fraction. By nature ring polymer conformational fluctuations are smaller due to the lack of free ends, so $\langle \delta \rangle$ for rings simply starts at a lower value. The end-free constraint is relevant in strong flows as well. For example, short linear polymers in the bidisperse blend can undergo end-over-end tumbling due to flow gradients in the z -direction while remaining significantly compressed in the y -direction (see Supplementary Information movie for an example at $f_S = 0.5, Wi_S = 3.5$). This conformational pathway is unavailable to rings, however, which retract weakly or rotate along their contours as seen in Fig. 13, but cannot undergo ‘end-over-end’ tumbling while fully compressed in the y -direction. Instead, rings must swell in the y -direction to completely tumble (Fig 12), a pathway that is suppressed by the compressional component of the applied planar extension.

Pure linear polymer solutions at matched contour length with the rings ($N_S = 75, N_R = 150$) are stretched to the same extension as rings at the same Wi . However, the bidisperse linear blend $f_S = 0.5$ is less stretched. Interestingly, a similar result is obtained in experiment for ring-linear blends at $f_R = 0.83$ vs $f_R = 0.5, 0.17$. We explain this result by the larger fluctuation quantity $\langle \delta \rangle$ for the bidisperse linear blends, which are close to the quantitative values for rings observed in experiment. At high Wi , chains cannot stretch far beyond their average extension due to finite extensibility. Therefore, conformational fluctuations at high Wi correspond to retractions. For sufficiently large $\langle \delta \rangle$, this results in a lower $\langle \Delta x/L \rangle_{ss}$.

The extensional viscosity of the pure linear solution $f_S = 1$ is slightly greater than the pure ring solution, while the 50/50 blends match quantitatively. This supports our previous conclusion that the stress arises from the polymer stretch. The small difference at $f_S = 1, f_R = 1$ is due to the difference in fractional extension, whereas for the blends the fractional extension matches. Intermolecular hooking is virtually absent in the bidisperse linear blends $f_S = 0.5$, supporting the conclusion that in both blends the increase in η_r with increasing fraction of $N_L = 150$ linear polymers is due to the higher stretch.

Overall, the bidisperse linear blend results show that the large conformational fluctuations we observe for the ring-linear case may be a more general feature in polymer solution blends and polydisperse solutions. Polydisperse solutions are often modeled with two-state models, where polymers are assumed to be either stretched or coiled based on their relaxation time, and intermolecular interactions are neglected. Our results show that intermolecular interactions in semidilute solutions under strong flows are not screened. In fact, they can lead to qualitatively different dynamics. The introduction of non-linear polymer architectures further complicates the issue. While

we observe topological constraints to be minimal in simulation, it is possible they play a more important role at higher molecular weight, as suggested by the larger $\langle \delta \rangle$ in experiment, and higher concentrations. Even in the absence of topological constraints, the effect of architecture is not trivial. Polymer size and shape play an important role which is challenging to predict *a priori* given the large concentration fluctuations present in semidilute solutions.

Further study is required to draw conclusions on the connection of bulk stress to the conformational dynamics observed here. Although the ring dynamics are surprising, they appear to have minimal influence on the extensional viscosity, which can be predicted by a simple linear interpolation between the pure ring and pure linear case via the chain restoring force. Exploration of a broader range of molecular weight and concentration may reveal structure-property relationships not observed here.

V. CONCLUSIONS

We have investigated the dynamics and rheology of ring-linear polymer blend solutions at the overlap concentration in planar extensional flow via Brownian dynamics simulations and single molecule experiments. Simulations and experiments both show that as the blend fraction of rings f_R decreases from a pure ring solution, the conformational fluctuations of the ring polymer portion of the blend increase. Simulations reveal that the origin of these dynamics are a combination of intermolecular topological and hydrodynamic interactions. We show that application of strong flows $Wi_R > 1$ can cause strong topological constraints in which a linear chain threads through a ring and forms an intermolecular ‘hook’ which strongly deforms the ring conformation. Equilibrium diffusion of rings at the overlap concentration is relatively insensitive to blend ratio, suggesting that flow introduces new dynamics. This is supported by the observation that pure linear solutions at $1 c^*$ form significantly fewer intermolecular hooks than ring-linear blends at $f_R = 0.83, 0.99$. Hooking leads overshoots in transient fractional extension on startup of flow for individual ring trajectories, which is quantified by conformational distributions. However, in simulation we find that the average number of hooks per chain upon startup of flow is low ($n_h < 0.05$), and once linear chains stretch fully at $\epsilon \approx 8$, hooking is nearly negligible. Considering that experiments show larger fluctuations, this effect could be sensitive to molecular weight and details of the flow geometry.

We show that steady state conformational fluctuations in simulation are driven by intermolecular HI. Three characteristic ring motions are observed: overstretching, retraction, and tank-treading. We measure the effective flow field due to the applied planar extensional flow plus the polymer disturbance velocity to explain these dynamics. We find that fluctuations in local concentration mod-

ify the flow and introduce regions of shear, rotational, and enhanced extensional flows that drive ring dynamics. We suggest that the flow modification is stronger for majority linear polymer blends because of the stronger restoring force, causing fluctuations to increase with decreasing blend fraction of rings. We directly test the influence of polymer architecture, size, and shape by comparing the ring-linear systems to bidisperse linear polymer blends in which ring polymers are replaced with linear chains of matched contour length. The dynamics of the short linear chains are in good qualitative and quantitative agreement with the rings. Thus, our simulations have broader relevance to polymer solution blends and polydisperse solutions in which intermolecular HI could drive unexpected dynamics.

The current work considered only solutions at $1 c^*$. The entanglement concentration for λ -DNA is $c_e \approx 3 c^*$, and for the simulation model we estimate $c_e \approx 8-10 c^*$. Despite this low concentration, we see emergent flow-induced topological constraints which could lead to entanglement dynamics below the equilibrium c_e . A potential area for future study is to quantify the crossover to entangled dynamics in non-equilibrium solutions with non-linear architectures. More generally, it is of interest to qualitatively characterize non-equilibrium conformations and solution stress in ring-linear blends above c^* , as equilibrium single molecule experiments suggest unique dynamics emerge compared to pure ring or pure linear solutions.^{30,31}

A more detailed understanding of the influence of intermolecular HI is also essential to elucidate the ring dynamics and bulk flow properties. While equilibrium scaling theories normally neglect intermolecular HI below c^* , there is considerable evidence from bulk rheology^{66,83,84} and molecular simulations,^{37,38,82} and theory⁸⁵ that as the pervaded volume of the polymer increases with strain rate, intermolecular interactions become relevant at concentrations significantly below c^* . Furthermore, a detailed study of flow-concentration coupling in connection to molecular dynamics is of interest. Here, we clearly show that spatiotemporal concentration fluctuations modify the effective flow and drive conformational dynamics. The motions observed at the molecular scale may also connect to elastic flow instabilities. More generally, instabilities in mixed flows^{86,87} and shear-induced demixing of entangled blends^{88,89} have also been reported. Recent developments in molecular simulation allow for unlimited strain accumulation in 2D mixed flows.^{90,91} Thus molecular simulations could provide a micromechanical mechanism for flow modification as well as detailed insight into the influence of macromolecular design variables including solvent quality, molecular weight, concentration, and chain architecture.

ACKNOWLEDGMENTS

This work was funded by the National Science Foundation under Grant No. CBET-1803757 for CES, a DuPont Science & Engineering fellowship for CDY, the National Science Foundation (NSF) Award CBET-1604038 for CMS and partially supported by the NSF through the University of Illinois at Urbana-Champaign Materials Research Science and Engineering Center (MRSEC) DMR-1720633 (YZ and CMS). The authors thank Sarit Dutta for helpful discussions.

- ¹M. Rubinstein, *Physical review letters* **57**, 3023 (1986).
- ²T. McLeish, *Science* **297**, 2005 (2002).
- ³J. A. Kaitz, C. E. Diesendruck, and J. S. Moore, *Journal of the American Chemical Society* **135**, 12755 (2013).
- ⁴E. M. Lloyd, H. Lopez Hernandez, A. M. Feinberg, M. Yourdkhani, E. K. Zen, E. B. Mejia, N. R. Sottos, J. S. Moore, and S. R. White, *Chemistry of Materials* **31**, 398 (2018).
- ⁵J.-W. Taanman, *Biochimica et Biophysica Acta (BBA)-Bioenergetics* **1410**, 103 (1999).
- ⁶M. Doi and S. F. Edwards, *The theory of polymer dynamics*, Vol. 73 (Oxford University Press, 1988).
- ⁷M. Rubinstein and R. H. Colby, *Polymer physics*, Vol. 23 (Oxford University Press, 2003).
- ⁸M. Kapnistos, M. Lang, D. Vlassopoulos, W. Pyckhout-Hintzen, D. Richter, D. Cho, T. Chang, and M. Rubinstein, *Nature materials* **7**, 997 (2008).
- ⁹J. D. Halverson, G. S. Grest, A. Y. Grosberg, and K. Kremer, *Physical review letters* **108**, 038301 (2012).
- ¹⁰T. Ge, S. Panyukov, and M. Rubinstein, *Macromolecules* **49**, 708 (2016).
- ¹¹Y. Doi, K. Matsubara, Y. Ohta, T. Nakano, D. Kawaguchi, Y. Takahashi, A. Takano, and Y. Matsushita, *Macromolecules* **48**, 3140 (2015).
- ¹²R. Pasquino, T. C. Vasilakopoulos, Y. C. Jeong, H. Lee, S. Rogers, G. Sakellariou, J. Allgaier, A. Takano, A. R. Brás, T. Chang, *et al.*, *ACS macro letters* **2**, 874 (2013).
- ¹³D. G. Tsalikis and V. G. Mavrantzas, *ACS Macro Letters* **3**, 763 (2014).
- ¹⁴Q. Huang, J. Ahn, D. Parisi, T. Chang, O. Hassager, S. Panyukov, M. Rubinstein, and D. Vlassopoulos, *Physical review letters* **122**, 208001 (2019).
- ¹⁵T. C. O'Connor, T. Ge, M. Rubinstein, and G. S. Grest, *Physical Review Letters* **124**, 027801 (2020).
- ¹⁶D. G. Tsalikis, V. G. Mavrantzas, and D. Vlassopoulos, *ACS Macro Letters* **5**, 755 (2016).
- ¹⁷A. J. Tsamopoulos, A. F. Katsarou, D. G. Tsalikis, and V. G. Mavrantzas, *Polymers* **11**, 1194 (2019).
- ¹⁸D. J. Mai, A. Saadat, B. Khomami, and C. M. Schroeder, *Macromolecules* **51**, 1507 (2018).
- ¹⁹C. M. Schroeder, *Journal of Rheology* **62**, 371 (2018).
- ²⁰R. M. Robertson, S. Laib, and D. E. Smith, *Proceedings of the National Academy of Sciences* **103**, 7310 (2006).
- ²¹O. Jagodzinski, E. Eisenriegler, and K. Kremer, *Journal de Physique I* **2**, 2243 (1992).
- ²²G. A. Hegde, J.-f. Chang, Y.-l. Chen, and R. Khare, *The Journal of chemical physics* **135**, 184901 (2011).
- ²³Y. Li, K.-W. Hsiao, C. A. Brockman, D. Y. Yates, R. M. Robertson-Anderson, J. A. Kornfield, M. J. San Francisco, C. M. Schroeder, and G. B. McKenna, *Macromolecules* **48**, 5997 (2015).
- ²⁴K.-W. Hsiao, C. M. Schroeder, and C. E. Sing, *Macromolecules* **49**, 1961 (2016).
- ²⁵C. M. Schroeder, R. E. Teixeira, E. S. Shaqfeh, and S. Chu, *Physical Review Letters* **95**, 018301 (2005).
- ²⁶W. Chen, J. Chen, and L. An, *Soft Matter* **9**, 4312 (2013).

- ²⁷M. Liebetreu, M. Ripoll, and C. N. Likos, *ACS Macro Letters* **7**, 447 (2018).
- ²⁸C. D. Young, J. R. Qian, M. Marvin, and C. E. Sing, *Physical Review E* **99**, 062502 (2019).
- ²⁹D. G. Tsalikis, T. S. Alexiou, P. V. Alatas, and V. G. Mavrantzas, *Macromolecular Theory and Simulations*, 2000016 (2020).
- ³⁰R. M. Robertson and D. E. Smith, *Macromolecules* **40**, 3373 (2007).
- ³¹C. D. Chapman, S. Shanbhag, D. E. Smith, and R. M. Robertson-Anderson, *Soft Matter* **8**, 9177 (2012).
- ³²Y. Zhou and C. M. Schroeder, *Physical Review Letters* **120**, 267801 (2018), arXiv:1805.06303.
- ³³S. Pan, D. A. Nguyen, T. Sridhar, P. Sunthar, and J. R. Prakash, *Journal of Rheology* **58**, 339 (2014).
- ³⁴Y. Zhou, K.-W. Hsiao, K. E. Regan, D. Kong, G. B. McKenna, R. M. Robertson-Anderson, and C. M. Schroeder, *Nature communications* **10**, 1753 (2019).
- ³⁵K.-W. Hsiao, C. Sasmal, J. Ravi Prakash, and C. M. Schroeder, *Journal of Rheology* **61**, 151 (2017).
- ³⁶C. Sasmal, K.-W. Hsiao, C. M. Schroeder, and J. Ravi Prakash, *Journal of Rheology* **61**, 169 (2017).
- ³⁷C. Stoltz, J. J. de Pablo, and M. D. Graham, *Journal of Rheology* **50**, 137 (2006).
- ³⁸C. D. Young and C. E. Sing, *The Journal of Chemical Physics* **151**, 124907 (2019).
- ³⁹C. M. Schroeder, E. S. Shaqfeh, and S. Chu, *Macromolecules* **37**, 9242 (2004).
- ⁴⁰C.-C. Huang, R. G. Winkler, G. Sutmman, and G. Gompper, *Macromolecules* **43**, 10107 (2010).
- ⁴¹C.-C. Huang, G. Sutmman, G. Gompper, and R. Winkler, *EPL (Europhysics Letters)* **93**, 54004 (2011).
- ⁴²A. Groisman and V. Steinberg, *Nature* **405**, 53 (2000).
- ⁴³E. S. Shaqfeh, *Annual Review of Fluid Mechanics* **28**, 129 (1996).
- ⁴⁴P. Pakdel and G. H. McKinley, *Physical Review Letters* **77**, 2459 (1996).
- ⁴⁵P. E. Arratia, C. Thomas, J. Diorio, and J. P. Gollub, *Physical review letters* **96**, 144502 (2006).
- ⁴⁶R. Poole, M. Alves, and P. J. Oliveira, *Physical review letters* **99**, 164503 (2007).
- ⁴⁷S. J. Haward, G. H. McKinley, and A. Q. Shen, *Scientific reports* **6**, 33029 (2016).
- ⁴⁸F. Cruz and M. Alves, *Physical Review Fluids* **3**, 113301 (2018).
- ⁴⁹N. Woo and E. S. Shaqfeh, *The Journal of chemical physics* **119**, 2908 (2003).
- ⁵⁰K. Kremer and G. S. Grest, *The Journal of Chemical Physics* **92**, 5057 (1990).
- ⁵¹J. Rotne and S. Prager, *The Journal of Chemical Physics* **50**, 4831 (1969).
- ⁵²H. Yamakawa, *The Journal of Chemical Physics* **53**, 436 (1970).
- ⁵³D. L. Ermak and J. McCammon, *The Journal of Chemical Physics* **69**, 1352 (1978).
- ⁵⁴M. Fixman, *Macromolecules* **19**, 1204 (1986).
- ⁵⁵T. Ando, E. Chow, Y. Saad, and J. Skolnick, *The Journal of Chemical Physics* **137**, 064106 (2012).
- ⁵⁶L. Miao, C. D. Young, and C. E. Sing, *The Journal of Chemical Physics* **147**, 024904 (2017).
- ⁵⁷C. D. Young, M. Marvin, and C. E. Sing, *The Journal of chemical physics* **149**, 174904 (2018).
- ⁵⁸A. Kraynik and D. Reinelt, *International journal of multiphase flow* **18**, 1045 (1992).
- ⁵⁹B. Todd and P. J. Davis, *Physical review letters* **81**, 1118 (1998).
- ⁶⁰M. H. N. Sefiddashti, B. J. Edwards, and B. Khomami, *Physical review letters* **121**, 247802 (2018).
- ⁶¹C. Beenakker, *The Journal of Chemical Physics* **85**, 1581 (1986).
- ⁶²A. Jain, P. Sunthar, B. Dünweg, and J. R. Prakash, *Physical Review E* **85**, 066703 (2012).
- ⁶³M. Dobson, I. Fox, and A. Saracino, *Journal of Computational Physics* **315**, 211 (2016).
- ⁶⁴T. Geyer and U. Winter, *The Journal of Chemical Physics* **130**, 114905 (2009).
- ⁶⁵Y. Zhou and C. M. Schroeder, *Macromolecules* **49**, 8018 (2016).
- ⁶⁶J. Dinic and V. Sharma, *Macromolecules* **53**, 4821 (2020).
- ⁶⁷J. F. Marko and E. D. Siggia, *Macromolecules* **28**, 8759 (1995).
- ⁶⁸P. T. Underhill and P. S. Doyle, *Journal of Rheology* **50**, 513 (2006).
- ⁶⁹A. Saadat and B. Khomami, *The Journal of Chemical Physics* **145**, 204902 (2016).
- ⁷⁰S. Kumar and R. G. Larson, *The Journal of Chemical Physics* **114**, 6937 (2001).
- ⁷¹A. E. Likhtman, *Macromolecules* **38**, 6128 (2005).
- ⁷²T. Uneyama and Y. Masubuchi, *The Journal of chemical physics* **137**, 154902 (2012).
- ⁷³A. Ramírez-Hernández, B. L. Peters, M. Andreev, J. D. Schieber, and J. J. de Pablo, *The Journal of chemical physics* **143**, 243147 (2015).
- ⁷⁴A. M. Fiore, F. Balboa Usabiaga, A. Donev, and J. W. Swan, *The Journal of Chemical Physics* **146**, 124116 (2017).
- ⁷⁵X. Liu and E. Chow, in *Parallel and Distributed Processing Symposium, 2014 IEEE 28th International (IEEE, 2014)* pp. 563–572.
- ⁷⁶A. Saadat and B. Khomami, *Physical Review E* **92**, 033307 (2015).
- ⁷⁷F. Cruz, R. Poole, A. Afonso, F. Pinho, P. Oliveira, and M. Alves, *Journal of Non-Newtonian Fluid Mechanics* **227**, 65 (2016).
- ⁷⁸P. Sousa, F. Pinho, M. Oliveira, and M. Alves, *Soft matter* **11**, 8856 (2015).
- ⁷⁹P.-G. de Gennes, *The Journal of Chemical Physics* **60**, 5030 (1974).
- ⁸⁰T. T. Perkins, D. E. Smith, and S. Chu, *Science* **276**, 2016 (1997).
- ⁸¹R. Larson, H. Hu, D. Smith, and S. Chu, *Journal of Rheology* **43**, 267 (1999).
- ⁸²R. Prabhakar, C. Sasmal, D. A. Nguyen, T. Sridhar, and J. R. Prakash, *Physical Review Fluids* **2**, 011301 (2017).
- ⁸³C. Clasen, J. Plog, W.-M. Kulicke, M. Owens, C. Macosko, L. Scriven, M. Verani, and G. H. McKinley, *Journal of Rheology* **50**, 849 (2006).
- ⁸⁴J. Dinic, M. Biagioli, and V. Sharma, *Journal of Polymer Science Part B: Polymer Physics* **55**, 1692 (2017).
- ⁸⁵R. Prabhakar, S. Gadkari, T. Gopesh, and M. Shaw, *Journal of Rheology* **60**, 345 (2016).
- ⁸⁶M. Cromer, G. H. Fredrickson, and L. Gary Leal, *Journal of Rheology* **61**, 711 (2017).
- ⁸⁷P. T. Corona, N. Ruocco, K. M. Weigandt, L. G. Leal, and M. E. Helgeson, *Scientific reports* **8**, 1 (2018).
- ⁸⁸I. Hindawi, J. Higgins, and R. Weiss, *Polymer* **33**, 2522 (1992).
- ⁸⁹J. D. Peterson, G. H. Fredrickson, and L. G. Leal, arXiv preprint arXiv:2002.04556 (2020).
- ⁹⁰T. A. Hunt, S. Bernardi, and B. Todd, *The Journal of chemical physics* **133**, 154116 (2010).
- ⁹¹A. Jain, C. Sasmal, R. Hartkamp, B. D. Todd, and J. R. Prakash, *Chemical Engineering Science* **121**, 245 (2015).